


RESEARCH PAPER



Hydrogen sulfide-induced GAPDH sulfhydrylation disrupts the CCAR2-SIRT1 interaction to initiate autophagy

Iram Khan Iqbal^a, Sapna Bajeli^a, Shivani Sahu^a, Shabir Ahmad Bhat^a, and Ashwani Kumar ^{a,b}

^aCouncil of Scientific and Industrial Research, Institute of Microbial Technology, Chandigarh, India; ^bAcademy of Scientific and Innovative Research (AcSIR), Ghaziabad, India

ABSTRACT

The deacetylase SIRT1 (sirtuin 1) has emerged as a major regulator of nucleocytoplasmic distribution of macroautophagy/autophagy marker MAP1LC3/LC3 (microtubule-associated protein 1 light chain 3). Activation of SIRT1 leads to the deacetylation of LC3 and its translocation from the nucleus into the cytoplasm leading to an increase in the autophagy flux. Notably, hydrogen sulfide (H₂S) is a cytoprotective gasotransmitter known to activate SIRT1 and autophagy; however, the underlying mechanism for both remains unknown. Herein, we demonstrate that H₂S sulfhydrates the active site cysteine of the glycolytic enzyme GAPDH (glyceraldehyde-3-phosphate dehydrogenase). Sulfhydrylation of GAPDH leads to its redistribution into the nucleus. Importantly, nuclear localization of GAPDH is critical for H₂S-mediated activation of autophagy as H₂S does not induce autophagy in cells with GAPDH ablation or cells overexpressing a GAPDH mutant lacking the active site cysteine. Importantly, we observed that nuclear GAPDH interacts with CCAR2/DBC1 (cell cycle activator and apoptosis regulator 2) inside the nucleus. CCAR2 interacts with the deacetylase SIRT1 to inhibit its activity. Interaction of GAPDH with CCAR2 disrupts the inhibitory effect of CCAR2 on SIRT1. Activated SIRT1 then deacetylates MAP1LC3B/LC3B (microtubule-associated protein 1 light chain 3 beta) to induce its translocation into the cytoplasm and activate autophagy. Additionally, we demonstrate this pathway's physiological role in autophagy-mediated trafficking of *Mycobacterium tuberculosis* into lysosomes to restrict intracellular mycobacteria growth. We think that the pathway described here could be involved in H₂S-mediated clearance of intracellular pathogens and other health benefits.

Abbreviations: ATG5: autophagy related 5; ATG7: autophagy related 7; BECN1: beclin 1, autophagy related; CCAR2/DBC1: cell cycle activator and apoptosis regulator 2; CFU: colony-forming units; DLG4/PSD95: discs large MAGUK scaffold protein 4; EX-527: 6-chloro-2,3,4,9-tetrahydro-1H-carbazole-1-carboxamide; GAPDH: glyceraldehyde-3-phosphate dehydrogenase; H₂S: hydrogen sulfide; HEK: human embryonic kidney cells; MAP1LC3B/LC3B: microtubule-associated protein 1 light chain 3 beta; MEF: mouse embryonic fibroblast; *Mtb*: *Mycobacterium tuberculosis*; MTOR: mechanistic target of rapamycin kinase; MOI: multiplicity of infection; NO: nitric oxide; PI3K: phosphatidylinositol-4,5-bisphosphate 3-kinase; PLA: proximity ligation assay; PRKAA: protein kinase, AMP-activated, alpha catalytic subunit; SIAH1: siah E3 ubiquitin protein ligase 1A; SIRT1: sirtuin 1; TB: tuberculosis; TP53INP2/DOR: transformation related protein 53 inducible nuclear protein 2; TRP53/TP53: transformation related protein 53

ARTICLE HISTORY

Received 22 November 2019
Revised 7 January 2021
Accepted 11 January 2021

KEYWORDS

Autophagy; CCAR2; GAPDH; hydrogen sulfide; *Mycobacterium tuberculosis*; PRKAA; SIRT1; starvation; sulfhydrylation; tuberculosis

Introduction

Hydrogen sulfide (H₂S) is a gasotransmitter analogous to nitric oxide (NO) and carbon monoxide (CO). Various cytoprotective functions, such as thermotolerance, antioxidant defense, vasorelaxation, neurotransmission, lifespan extension, autophagy induction, etc., are ascribed to H₂S [1]. H₂S primarily functions through S-sulfhydrylation or persulfhydrylation of cysteine residues on proteins to modulate their function [2,3]. GAPDH (glyceraldehyde-3-phosphate dehydrogenase) and actin are the most abundant proteins that are sulfhydrated by H₂S [4]. Sulfhydrylation of GAPDH at the active site cysteine (C150) induces its enzymatic activity [4] and stabilizes its interaction with the E3 ubiquitin ligase SIAH1 (seven in absentia homolog 1), which enables

degradation of PSD95 (postsynaptic density 95 protein) and results in memory impairment [5]. Importantly, GAPDH can be nitrosylated at C150, which induces its translocation into the nucleus [6], wherein it S-transnitrosylates and inactivates the NAD⁺ dependent deacetylase SIRT1 (sirtuin 1) [7]. Interestingly, H₂S also induces expression [8] and activity [9] of SIRT1. Increased SIRT1 activity imparts a plethora of health benefits, including retardation of cellular senescence and aging, aversion of metabolic diseases, cancer, cardiac aging, neurodegeneration, etc [10]. However, the molecular basis of the H₂S-mediated increase in SIRT1 activity remains poorly defined.

Several benefits associated with H₂S are also attributed to macroautophagy (hereafter referred to as autophagy). Autophagy is a cytoprotective process through which damaged organelles, intracellular pathogens, etc., are sequestered within a double membrane structure called the autophagosome, which then fuses with lysosomes to facilitate degradation and recycling of the sequestered material. Importantly, antigen-presenting cells such as macrophages and dendritic cells utilize autophagy for the trafficking of pathogens to lysosomes and thus their clearance [11]. Besides eliminating pathogens, autophagy plays a critical role in regulating innate and adaptive immune responses and therefore dictates the outcome of several infectious diseases such as tuberculosis [12–15]. It also plays an essential role in interferon-gamma mediated restriction of growth of intracellular *Mycobacterium* [16]. Besides, the regulation of the immune response and eliminating pathogens, it plays a vital role in cellular homeostasis. Since autophagy is essential for cellular homeostasis, its initiation, elongation, and maturation of autophagosomes are tightly regulated [17]. Some of the proteins involved in autophagy initiation, such as ATG5, ATG7, and MAP1LC3/LC3 (microtubule-associated protein 1 light chain 3; a mammalian homolog of yeast Atg8), reside inside the nucleus in acetylated form. Upon glucose starvation, PRKAA (protein kinase, AMP-activated, alpha catalytic subunit; a subunit of AMP-activated protein kinase, AMPK) phosphorylates GAPDH on serine 122 (serine 120 in mice). It induces redistribution of GAPDH into the nucleus, where it interacts with SIRT1. This interaction leads to the activation of SIRT1 through the displacement of the SIRT1 inhibitor, CCAR2/DBC1 (cell cycle activator and apoptosis regulator 2) from the SIRT1-CCAR2 complex [18]. Activation of SIRT1 leads to the deacetylation of ATG5, ATG7, and LC3. This deacetylation enables the interaction of these proteins with the TP53INP2 (transformation related protein 53 inducible nuclear protein 2). TP53INP2 facilitates the movement of LC3 from the nucleus to the cytoplasm, where it is conjugated with phosphatidylethanolamine and plays a critical role in autophagosome formation [19]. Recent studies indicate that H₂S induces autophagy [20,21]. However, the molecular basis of autophagy regulation by H₂S remains elusive. Given that H₂S induces SIRT1 activity and sulfhydrates GAPDH directly, the GAPDH-SIRT1-LC3 axis's role in the modulation of autophagy by H₂S could be analyzed.

In this study, we utilized immunofluorescence microscopy, subcellular fractionation, and transient expression of GFP-tagged GAPDH to demonstrate that GAPDH translocates to the nucleus in response to H₂S exposure. Furthermore, several assays were utilized to elucidate the role of GAPDH in autophagy modulation by H₂S. Several independent approaches were employed to demonstrate the interaction between GAPDH with CCAR2, ultimately leading to the activation of SIRT1 and autophagy. We think that this work has identified a sulfhydrated-

GAPDH-CCAR2-SIRT1 signaling axis that regulates autophagy in response to H₂S.

Results

Hydrogen sulfide-induced autophagy modulates trafficking and survival of Mycobacterium tuberculosis (Mtb) inside macrophages

H₂S has been reported to modulate autophagy. Few reports indicate that H₂S induces autophagy [21,22], while others suggest a negative correlation of H₂S with autophagy [23,24]. This difference could be due to the use of different cell lines and different concentrations of H₂S through distinct donors in various studies. So we began with assessing whether H₂S modulates autophagy in macrophages. Several H₂S donors are available for studying its biological function [25,26]. We treated various cell lines with H₂S donor GYY4137. GYY4137 was used as an H₂S donor in these experiments since it is water-soluble and releases H₂S slowly [27]. We analyzed H₂S mediated changes in lipidation of LC3B by western blotting. Lipidation of LC3B is considered a key biomarker for measuring autophagic flux [28]. We found an increase in the lipidated LC3B-II form (as normalized to ACTB/ β -actin levels) upon H₂S treatment in RAW 264.7 macrophages, human embryonic kidney cells (HEK) 293 T, and mouse embryonic fibroblasts (MEFs) (Figure 1A). Moreover, treatment with bafilomycin A₁ in combination with the H₂S donor increased LC3B lipidation compared to bafilomycin A₁ alone (Figure 1A), suggesting an increase in autophagy flux rather than inhibition of autophagy. Furthermore, we tested whether H₂S modulates autophagy in primary macrophages. H₂S induced autophagy in bone marrow-derived macrophages (BMDMs) (Figure S1A). We confirmed these results by overexpression of ptfLC3 in RAW 264.7 macrophages, which simultaneously measures autophagosome formation and maturation [29]. We observed that H₂S exposure leads to increased autophagic flux (Figure 1B–D and S1B). These observations were verified using a GFP-LC3 construct as well (Figure S1C–E). The possibility of GFP aggregation upon overexpression was ruled out using an LC3 mutant, LC3- Δ G120, defective in punctae-formation [30] (Figure S1F). Next, to test whether H₂S-induced autophagy is canonical, we treated cells with H₂S in the presence of wortmannin, a known phosphatidylinositol-4,5-bisphosphate 3-kinase (PI3K) inhibitor. We found that wortmannin inhibited H₂S-induced autophagy, suggesting that H₂S induces autophagy via the canonical pathway (Figure S1G). Furthermore, DQ™ Red BSA was used to demonstrate that H₂S induces autolysosome maturation (Figure S1H). Earlier studies have shown that H₂S could induce apoptosis through the activation of TP53 [31]. Thus, we tested whether the concentration of H₂S used herein, induces apoptosis. We observed that the concentrations (250–500 μ M of GYY4137) of H₂S used in this study do not induce apoptosis (Figure S1I). We also analyzed whether the increase in autophagy flux results in a decrease in the levels of SQSTM1, which is used as

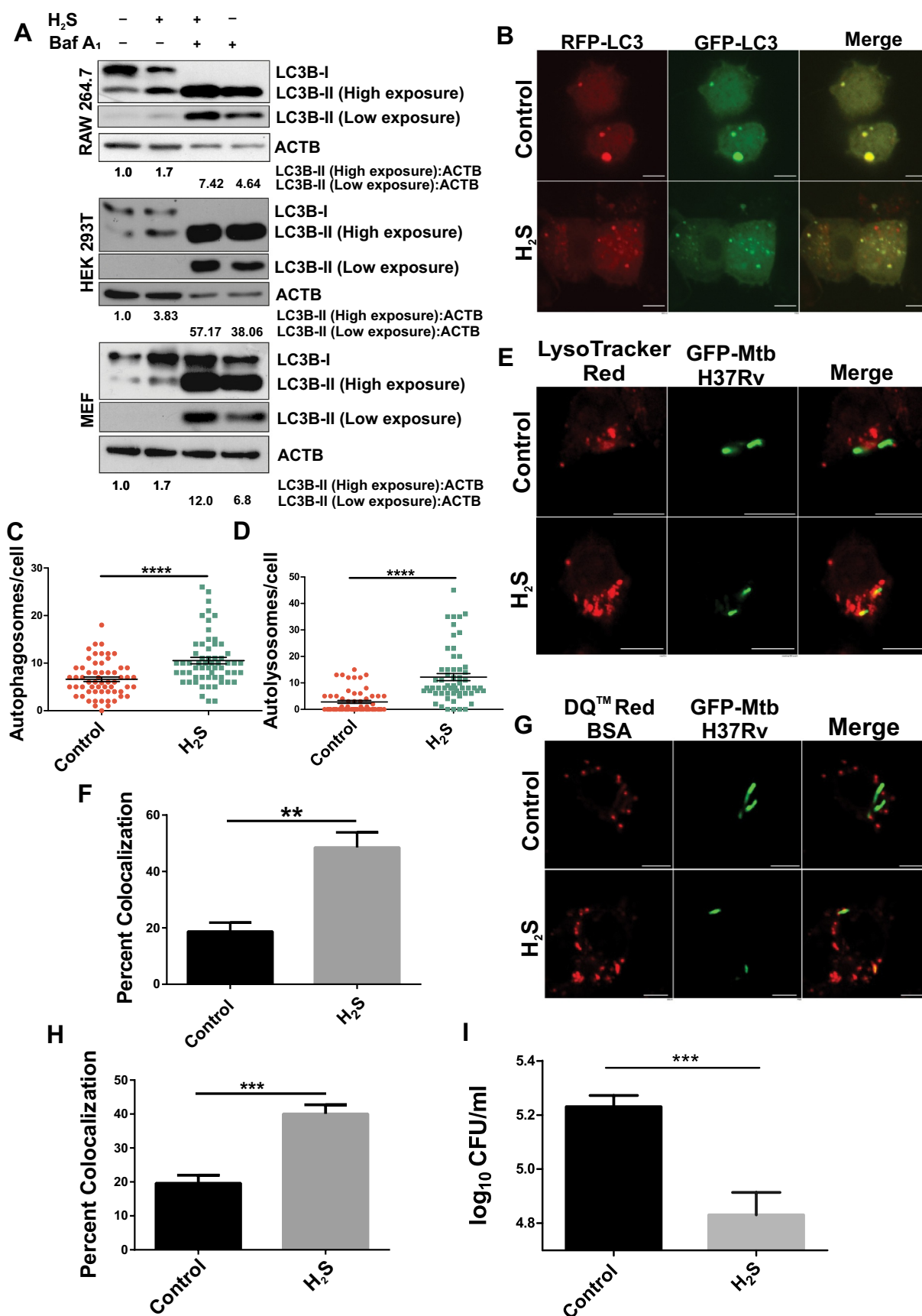


Figure 1. Hydrogen sulfide-induced autophagy modulates trafficking and survival of *Mtb* inside macrophages. (A) RAW 264.7 macrophages, HEK 293 T cells, and MEF cells were pre-treated with bafilomycin A₁ (Baf A₁, 100 nM) for 2 h followed by treatment with H₂S for 2 h. Western blotting was performed to analyze the LC3 flux. Western blotting was performed to measure LC3B lipidation. ACTB was used for normalization. The numbers below lanes indicate the fold change of LC3B-II relative to the ACTB signal calculated by performing densitometric analysis using ImageJ software. (B) RAW 264.7 macrophages transiently expressing ptfLC3 were treated with H₂S for 2 h and imaged using a confocal microscope. (C) An average number of autophagosomes per cell, as in (B), was quantified using ImageJ. (D) An average

number of autolysosomes per cell, as in (B), was quantified using ImageJ. Data (in C and D) represent the mean \pm SEM from 3 independent experiments ($n = 60$; 20 randomly chosen cells from each experiment were quantified). Statistical significance was determined using Student's *t*-test. (E) RAW 264.7 macrophages were infected with GFP-*Mtb* H37Rv at an MOI of 1:5 and treated with H₂S or control buffer for 2 h. Lysosomes were visualized using LysoTracker[®] Red and imaged using confocal microscopy. (F) Percent colocalization of GFP-*Mtb* H37Rv with LysoTracker[®] Red was calculated using ImageJ. Data represent the mean \pm SEM from 3 independent experiments ($n = 180$; 60 randomly chosen cells from each experiment were quantified). Statistical significance was determined using Student's *t*-test. (G) RAW 264.7 macrophages infected with GFP-*Mtb* H37Rv at an MOI of 1:5 were pulsed with DQ[™] Red BSA for 20 min and washed to remove the excess. Cells were treated with H₂S or control buffer for 2 h and fixed using 4% PFA. Cells were imaged using confocal microscopy. (H) Percent colocalization of GFP-*Mtb* H37Rv with DQ[™] Red BSA was calculated using ImageJ. Data represent the mean \pm SEM from 3 independent experiments ($n = 150$; 50 randomly chosen cells from each experiment were quantified). Statistical significance was determined using Student's *t*-test. (I) *Mtb* H37Rv survival in RAW 264.7 macrophages upon 250 μ M GYY4137 treatment for 2 h was calculated using CFU estimation. Data represent mean \pm SEM from 3 independent experiments. Statistical significance was determined using Student's *t*-test. ** indicates a *P* value of <0.01, *** indicates a *P* value of <0.001 and **** represents a *P* value of <0.0001. Scale bar: 5 μ m.

another marker of autophagy [32]. We did not observe any change in the SQSTM1 levels upon the exposure of H₂S (Figure S1J).

Mycobacterium tuberculosis (*Mtb*) arrests the maturation of autophagosomes and inhibits their fusion with lysosomes. Activation of macrophages through cytokines such as interferon-gamma is known to activate autophagy [16,33]. Induction of autophagy facilitates the maturation of phagosomes and fusion with lysosomes to restrict the growth of intracellular *Mtb* [16,33]. Interestingly, innate immunity regulator TBK1 (TANK binding kinase 1) [34] and ubiquitin ligase parkin [35] play an important role in autophagic response to TB infection. To establish the physiological relevance of H₂S-induced autophagy, we analyzed whether it modulates the trafficking of *Mtb* to lysosomes and its intracellular survival. We infected RAW 264.7 macrophages with *Mtb* expressing GFP (GFP-*Mtb* H37Rv) and used LysoTracker[®] Red to visualize the lysosomes. We observed that H₂S-mediated induction of autophagy overcame the blockade of autophagosome-lysosome fusion induced by *Mtb* (Figure 1E,F). ~ 2.5-fold increase in the localization of *Mtb* cells with lysosomes was observed in H₂S treated macrophages compared to untreated cells (Figure 1E,F). Furthermore, we also utilized the DQ[™] Red BSA to visualize the active lysosomes and observed an increase in *Mtb*'s localization into functional lysosomes in H₂S stimulated cells compared to untreated cells (Figure 1G,H). Since the localization of *Mtb* cells to the lysosomes is associated with decreased survival of *Mtb*, we analyzed whether H₂S exposure of macrophages could reduce the survival of intracellular *Mtb*. As anticipated, we observed a significant reduction in intracellular *Mtb* survival in the H₂S treated macrophages compared with untreated macrophages (Figure 1I). It is possible that H₂S could directly inhibit the mycobacterial growth through inhibition of respiration. Thus we exposed exponential phase cultures of *Mtb* to H₂S for 72 h and measured the mycobacterial survival. We did not observe inhibition of mycobacterial growth by H₂S (Figure S1K).

Hydrogen sulfide induces nuclear translocation of GAPDH through sulfhydrylation

Earlier studies have suggested that GAPDH is one of the significant targets of H₂S mediated sulfhydrylation [4]. Thus we tested whether concentrations used in this study induce sulfhydrylation on GAPDH. Toward this, we utilized a modified biotin switch assay [4] and validated that H₂S exposure leads to sulfhydrylation of GAPDH (Figure 2A). Earlier studies have

indicated that nitrosylation of GAPDH induces its nuclear localization. However, the effect of sulfhydrylation on the subcellular localization of mammalian GAPDH is not known. We hypothesized that H₂S modulates the subcellular localization of GAPDH. To test this hypothesis, we examined the subcellular localization of GAPDH upon exposure of macrophages with H₂S using starvation as a positive control to visualize the nuclear translocation of GAPDH. Immuno-staining for endogenous GAPDH demonstrated that H₂S exposure results in translocation of GAPDH into the nucleus similar to starvation (Figure 2B and C). These findings were confirmed by transiently expressing GFP tagged GAPDH in RAW 264.7 macrophages (Figure 2D and E). To determine whether the same is true for human origin cells, we transiently expressed GFP-tagged GAPDH in HEK 293 cells and treated them with H₂S. We observed significant nuclear localization of GAPDH in response to exogenous H₂S exposure in these cells as well (Figure S2A and B). These results were validated by subcellular fractionation of HEK 293 cells exposed to H₂S. We observed higher levels of GAPDH in the nuclear fractions from H₂S-treated cells (Figure 2F). Cell fractionation in RAW 264.7 macrophages also confirmed that H₂S induces nuclear translocation of GAPDH (Figure S2C). We also analyzed whether this increase in nuclear GAPDH is due to increased expression of GAPDH. Western blot analysis suggested that H₂S does not induce the expression of GAPDH (Figure S2D). Next, we analyzed whether the nuclear localization of GAPDH upon H₂S exposure is reversible or not. Toward this, the RAW 264.7 macrophages were exposed to H₂S for two hours, washed with PBS, and then incubated with fresh medium without the H₂S donor for another two hours. Immuno-staining for endogenous GAPDH after removing H₂S demonstrated the redistribution of GAPDH from the nucleus to the cytoplasm (Figure 2G and H), suggesting that GAPDH translocation to the nucleus is a reversible and dynamic process.

Sulfhydrylation of active site cysteine is critical for nuclear translocation of GAPDH

Our studies have suggested that H₂S sulfhydrates GAPDH. We next analyzed whether the active site cysteine (C150) of GAPDH is the primary target for sulfhydrylation. Toward this, we employed the protein persulfide detection protocol (ProPerDP) that directly measures the sulfhydrylation of a protein [36]. We overexpressed FLAG-tagged WT GAPDH and GAPDH^{C150S} in HEK 293 T cells. The cells were exposed to H₂S, and sulfhydrylation of GAPDH was determined using

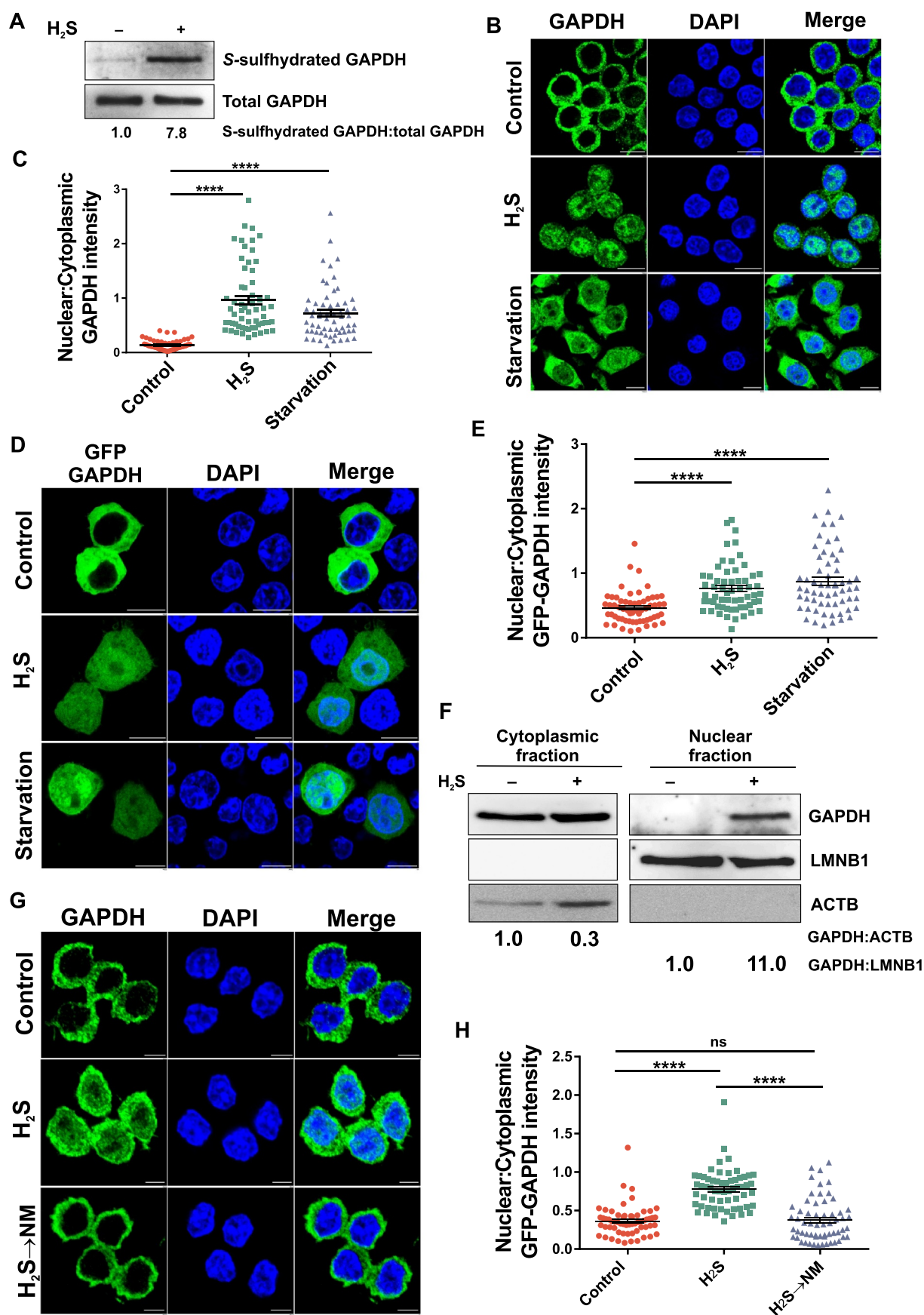


Figure 2. Hydrogen sulfide induces nuclear translocation of GAPDH through sulfhydration. (A) Biotin-switch assay was performed, and S-sulphydrated GAPDH was detected through western blotting in HEK293 cells. Total GAPDH was used for normalization. Numbers below lanes indicate the fold change of S-sulphydrated GAPDH relative to the total GAPDH signal calculated using ImageJ. (B) Representative confocal images of the intracellular distribution of GAPDH in RAW 264.7 macrophages independently treated with H₂S, control buffer, or starved for 2 h, followed by staining with anti-GAPDH antibody (green). Cell nuclei were counterstained with DAPI (blue). (C) Quantification of the nuclear:cytoplasmic ratio of GAPDH for the experiment described in (B) using ImageJ software. Data represent mean ± SEM from 3

independent experiments ($n = 60$; 20 randomly chosen cells from each experiment were quantified). Statistical significance was determined using Student's *t*-test. (D) Representative confocal images of the distribution of GFP-GAPDH overexpressed in RAW 264.7 cells. RAW 264.7 cells were treated with H₂S or starved for 2 h, followed by staining with DAPI (blue) to visualize nuclei. (E) Quantification of nuclear/cytoplasmic GAPDH using ImageJ software for the experiment described in (D). Data represent mean \pm SEM from 3 independent experiments ($n = 60$; 20 randomly chosen cells from each experiment were quantified). Statistical significance was determined using Student's *t*-test. (F) Western blots of subcellular fractions from HEK 293 cells treated with H₂S or their control. LMNB1 and ACTB were used as markers for nuclear and cytoplasmic fractions, respectively. The numbers below lanes indicate the fold change calculated using the densitometric analysis of GAPDH relative to the ACTB signal in cytoplasmic fraction and LMNB1 signal in nuclear fraction using ImageJ software. (G) Representative confocal images of the intracellular distribution of GAPDH in RAW 264.7 macrophages independently treated with H₂S or control buffer for 2 h and cells treated with H₂S for 2 h followed by washing and supplementation of fresh normal media (NM) for 2 h. Cells were stained with anti-GAPDH antibody (green), and cell nuclei were counterstained with DAPI (blue). (H) Quantification of the nuclear:cytoplasmic ratio of GAPDH for the experiment described in (G) using ImageJ software. Data represent mean \pm SEM from 3 independent experiments ($n = 60$; 20 randomly chosen cells from each experiment were quantified). Statistical significance was determined using Student's *t*-test. **** indicates a *P* value of <0.0001 . Scale bar: 5 μ m.

the ProPerDP. These experiments suggest that H₂S mediated sulfhydrylation primarily happens at the active site cysteine (Figure 3A). Next, we analyzed whether sulfhydrylation of C150 is critical for H₂S mediated nuclear translocation of GAPDH. Toward this, we analyzed the subcellular localization of GFP-tagged WT GAPDH and GAPDH^{C150S} in response to H₂S, where starvation was used as a positive control. Importantly, we observed that although GFP-WT GAPDH localizes to the nucleus, the GAPDH^{C150S} variant of GAPDH does not translocate into the nucleus (Figure 3B,C). Since serine can fuse with homocysteine during cysteine biosynthesis [37], we also utilized the GAPDH^{C150A} to study the role of sulfhydrylation in nuclear translocation of GAPDH. We observed that in line with the earlier observations, the GAPDH^{C150A} could not translocate into the nucleus (Figure 3D,E). Collectively these observations suggest that sulfhydrylation of GAPDH at C150 is critical for its nuclear localization in response to H₂S.

Sulfhydrylation of GAPDH active site cysteine is critical for hydrogen sulfide-induced autophagy

Recently, GAPDH was shown to regulate starvation-induced autophagy [18]. Thus, we assessed whether GAPDH plays a role in the induction of autophagy by H₂S. To this end, we silenced *Gapdh* in RAW 264.7 macrophages and exposed them to H₂S. We observed that in cells with *Gapdh* knock-down, H₂S was unable to induce autophagy as deduced through western blot analysis for lipidation of LC3B (Figure 4A). These findings were confirmed through confocal microscopy-based visualization of GFP-LC3 puncta formation (Figure 4B,C). To verify that these changes are primarily due to the sulfhydrylation of GAPDH at the active site cysteine by H₂S, we overexpressed the GAPDH^{C150S} in RAW 264.7 cells. In these cells, the capability of H₂S to induce autophagy was attenuated as observed by lipidation of LC3B (Figure 4D) and formation of LC3B puncta (Figure 4E,F). The critical role of sulfhydrylation of GAPDH at cysteine 150 in H₂S mediated induction of autophagy was further validated using the GAPDH^{C150A} (Figure 4G,H). Since the above findings suggest that sulfhydrylation of active site cysteine is critical for nuclear localization of GAPDH and activation of autophagy, we hypothesized that in cells overexpressing GAPDH tagged with a nuclear exclusion signal (GAPDH-NES), H₂S would be unable to induce autophagy. Indeed, we observed that H₂S failed to induce autophagy in cells overexpressing NES-GAPDH (Figure S3A and B). In light of these findings, we

also tested whether overexpression of GAPDH with a nuclear localization signal (GAPDH-NLS) activates autophagy. We observed that the nuclear localization of GAPDH alone is not sufficient for the induction of autophagy (Figure S3C and D). These observations suggest that sulfhydrylation of GAPDH in the cytoplasm is important for the induction of autophagy.

Hydrogen sulfide-mediated induction of autophagy does not depend upon activation of PRKAA

An elegant study earlier demonstrated that GAPDH is phosphorylated on serine 120 by activated PRKAA in response to glucose starvation [18]. This phosphorylation induces the translocation of GAPDH into the nucleus. Thus, we hypothesized that upon stimulation of cells with H₂S, PRKAA would be activated to phosphorylate GAPDH and mediate its nuclear translocation, subsequently leading to autophagy induction. To test this hypothesis, we assessed whether H₂S treatment leads to phosphorylation and activation of PRKAA. We treated RAW 264.7 macrophages with the H₂S donor GYY4137 and measured phosphorylation of PRKAA. We did not observe any noticeable increase in the levels of phospho-PRKAA upon treatment with H₂S (Figure S4A). We also analyzed whether H₂S induces nuclear localization of GAPDH in the presence of compound C (also known as dorsomorphin), an established PRKAA inhibitor. To this end, we utilized GFP-tagged GAPDH. To our surprise, we observed that GAPDH translocates to the nucleus upon exposure to H₂S, even in the presence of compound C, suggesting that H₂S-induced nuclear localization of GAPDH occurs independently of PRKAA (Figure 5A,B). Since PRKAA-mediated phosphorylation of GAPDH at serine 120 is critical for its nuclear translocation in response to starvation, we analyzed whether GAPDH^{S120A} translocates to the nucleus upon H₂S treatment. We observed that GAPDH^{S120A} translocates to the nucleus upon treatment with H₂S (Figure 5C,D), while it does not translocate to the nucleus upon starvation, as demonstrated previously [18]. We further analyzed whether H₂S-induced autophagy is altered by inhibition of PRKAA via monitoring lipidation of LC3B (Figure 5E). These observations were confirmed using siRNA for *Prkaa1* (Figure 5F). Furthermore, we utilized the LC3 mCherry probe for monitoring autophagy in cells wherein *Prkaa1* was knocked down (Figure 5G,H). Additionally, we also observed that H₂S induces LC3 punctae formation in cells overexpressing the GAPDH^{S120A} variant (Figure 5I,J). In sum, these observations

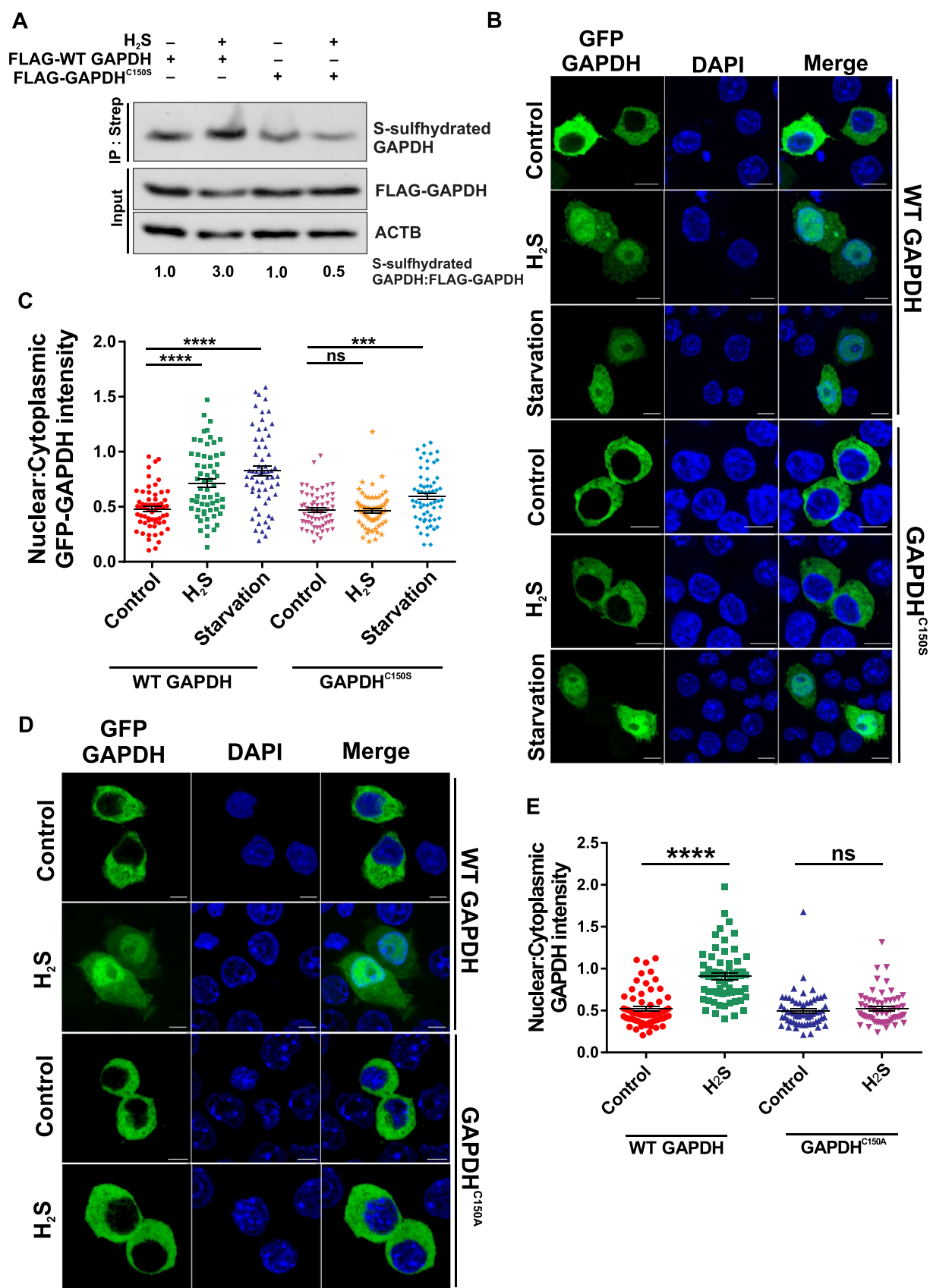


Figure 3. Sulfhydration of active site cysteine is critical for nuclear translocation of GAPDH (A) S-sulfhydrated GAPDH was detected using protein persulfide detection protocol. Sulfhydrated GAPDH was labeled with Iodoacetyl-PEG₂-Biotin and biotinylated S-sulfhydrated GAPDH was pulled down using streptavidin agarose beads, followed by its detection using western blotting in HEK293T cells. Numbers below lanes indicate the fold change of S-sulfhydrated GAPDH relative to the FLAG-GAPDH signal in input calculated by the densitometric analysis using ImageJ software. (B) Representative confocal images for analysis of the distribution of GAPDH in the nucleus and cytoplasm. RAW 264.7 macrophages transiently overexpressing GFP- WT GAPDH or GFP-GAPDH^{C150S} were treated with H₂S donor, control buffer, or starved for 2 h followed by staining with DAPI. (C) Quantification of GAPDH nuclear:cytoplasmic ratio in RAW 264.7 macrophages transiently overexpressing

GFP- WT GAPDH or GFP-GAPDH^{C150S} using ImageJ software on experiments described in (B). Data represent mean \pm SEM from 3 independent experiments ($n = 60$; 20 randomly chosen cells from each experiment were quantified). Statistical significance was determined using Student's *t*-test. (D) Representative confocal images for analysis of the distribution of GAPDH in the nucleus and cytoplasm. RAW 264.7 macrophages transiently overexpressing GFP- WT GAPDH or GFP-GAPDH^{C150A} were treated with H₂S donor or control buffer and followed by staining with DAPI. (E) Quantification of GAPDH nuclear:cytoplasmic ratio in RAW 264.7 macrophages transiently overexpressing GFP- WT GAPDH or GFP-GAPDH^{C150A} using ImageJ software on experiments described in (D). Data represent mean \pm SEM from 3 independent experiments ($n = 60$; 20 randomly chosen cells from each experiment were quantified). Statistical significance was determined using Student's *t*-test. *** indicates a *P* value of <0.001 and **** represents a *P* value of <0.0001 . Scale bar: 5 μ m.

suggest PRKAA mediated phosphorylation of GAPDH at S120 is not critical for H₂S mediated autophagy induction. H₂S can inhibit mitochondrial respiration at high concentrations, while at low concentrations, it induces cellular bioenergetics and increases cellular ATP [1]. Since depletion of ATP leads to the activation of PRKAA via STK11/LKB1, we also analyzed cellular ATP levels using a genetically encoded biosensor, Perceval-HR [38]. We observed that the concentration of H₂S used in this study leads to the activation of cellular energetics and increased ATP levels (Figure S4B). These observations suggest that H₂S increases cellular ATP and that autophagy induced by H₂S is not dependent on PRKAA.

SIRT1 is essential for hydrogen sulfide-induced autophagy

SIRT1 plays a critical role in starvation-induced autophagy [19]. Significantly, SIRT1 catalyzes the deacetylation of the autophagic proteins LC3, ATG7, and ATG5. Under normal conditions, the activity of SIRT1 is inhibited by CCAR2, while during glucose starvation, GAPDH interacts with SIRT1 and relieves the inhibition of CCAR2 [18]. To determine whether SIRT1 is also essential for H₂S-induced autophagy, we employed a SIRT1 specific inhibitor, EX-527. Pretreatment with EX-527 inhibited H₂S-induced lipidation of LC3B (Figure 6A). Genetic ablation of *Sirt1* through siRNA demonstrated that H₂S-induced autophagy is dependent on SIRT1 (Figure 6B). These findings were confirmed using the GFP-RFP-LC3 probe, suggesting that H₂S cannot induce autophagy if SIRT1 is inhibited (Figure 6C-E). Analysis with GFP-LC3 suggested a role for SIRT1 in the induction of autophagy by H₂S (Figure S5A). Furthermore, we found that SIRT1 inhibitor EX-527 inhibits H₂S-induced maturation of autolysosomes using DQ™ Red BSA (Figure S5B). Since LC3, ATG7, and ATG5 interact with SIRT1 and are its substrates, we examined whether SIRT1 also interacts with ATG proteins during H₂S-induced autophagy. We found an increase in the interaction of SIRT1 and LC3 in the presence of H₂S, and inhibition of SIRT1 activity using EX-527 abrogates this interaction (Figure 6F). Two other critical autophagic proteins, ATG5 and ATG7, also interact with SIRT1 upon exposure to H₂S (Figure S5C and D). Earlier studies have demonstrated that upon starvation, SIRT1 is activated, and it catalyzes the deacetylation of LC3 [19]. This enables the interaction of LC3 with TP53INP2 and its export from the nucleus into the cytoplasm. Since H₂S induces the interaction of SIRT1 with LC3, it would perhaps induce its deacetylation to facilitate its export from the nucleus to the cytoplasm. Treatment of H₂S caused the export of LC3 from the nucleus to the cytoplasm (Figure 6G). We also analyzed if this translocation of LC3 into the cytoplasm is dependent on sulfhydrylation of GAPDH. We observed that H₂

S is attenuated for inducing translocation of LC3 into the cytoplasm in the RAW 264.7 macrophages overexpressing the GAPDH^{C150S} (Figure 6H).

Next, we examined whether SIRT1 has any role in H₂S-mediated trafficking of *Mtb* into lysosomes or regulating its intracellular growth. To this end, we infected RAW 264.7 macrophages with GFP-*Mtb* H37Rv. LysoTracker® Red was used to visualize lysosomes in these experiments. We observed that macrophages treated with the SIRT1 inhibitor EX-527 exhibited significantly attenuated trafficking of *Mtb* cells into lysosomes in response to H₂S exposure (Figure 6I,J). We also utilized DQ™ Red BSA for visualizing active lysosomes (Figure S5E). Next, we analyzed whether SIRT1 is required for H₂S-mediated clearance of *Mtb* cells. Estimation of surviving intracellular *Mtb* cells suggested that the capability of H₂S to retard intracellular mycobacterial growth is attenuated upon inhibition of SIRT1 function by EX-527 (Figure 6K). These findings indicate that H₂S-mediated induction of autophagy and control of mycobacterial growth depends on the function of SIRT1.

Hydrogen sulfide induces the interaction of GAPDH with CCAR2

A recent study has suggested that GAPDH localizes to the nucleus and directly interacts with SIRT1 during glucose starvation [18]. The experiments described above indicated that H₂S induces SIRT1 activity. Thus, we analyzed whether sulfhydrylated GAPDH interacts with SIRT1. To this end, we performed pull-down assays and studied protein-protein interactions. In co-immunoprecipitation experiments, we did not observe any interaction between SIRT1 and GAPDH upon H₂S exposure. We think that this might be due to a weak interaction, if any, between GAPDH and SIRT1. Given that H₂S does not induce an interaction between GAPDH and SIRT1 but activates SIRT1-mediated deacetylation, we hypothesized that sulfhydrylated GAPDH interacts with CCAR2, an inhibitor of SIRT1 function. To test this hypothesis, we performed co-immunoprecipitation experiments in H₂S-treated and untreated cells. We observed a robust interaction of GAPDH with CCAR2 in H₂S-treated HEK 293 T (Figure 7A) and MEF cells (Figure S6A). Importantly, this interaction was detected with endogenous GAPDH and CCAR2 as well (Figure 7B). To quantify the strength of interaction, we utilized the proximity ligation assay (PLA). PLA allows quantitative measurement of the interaction between two proteins at endogenous expression levels. In these experiments, we observed a high-affinity interaction between CCAR2 and GAPDH (Figure 7C,D). In agreement with our earlier observations, we did not detect an interaction between GAPDH and SIRT1 in response to

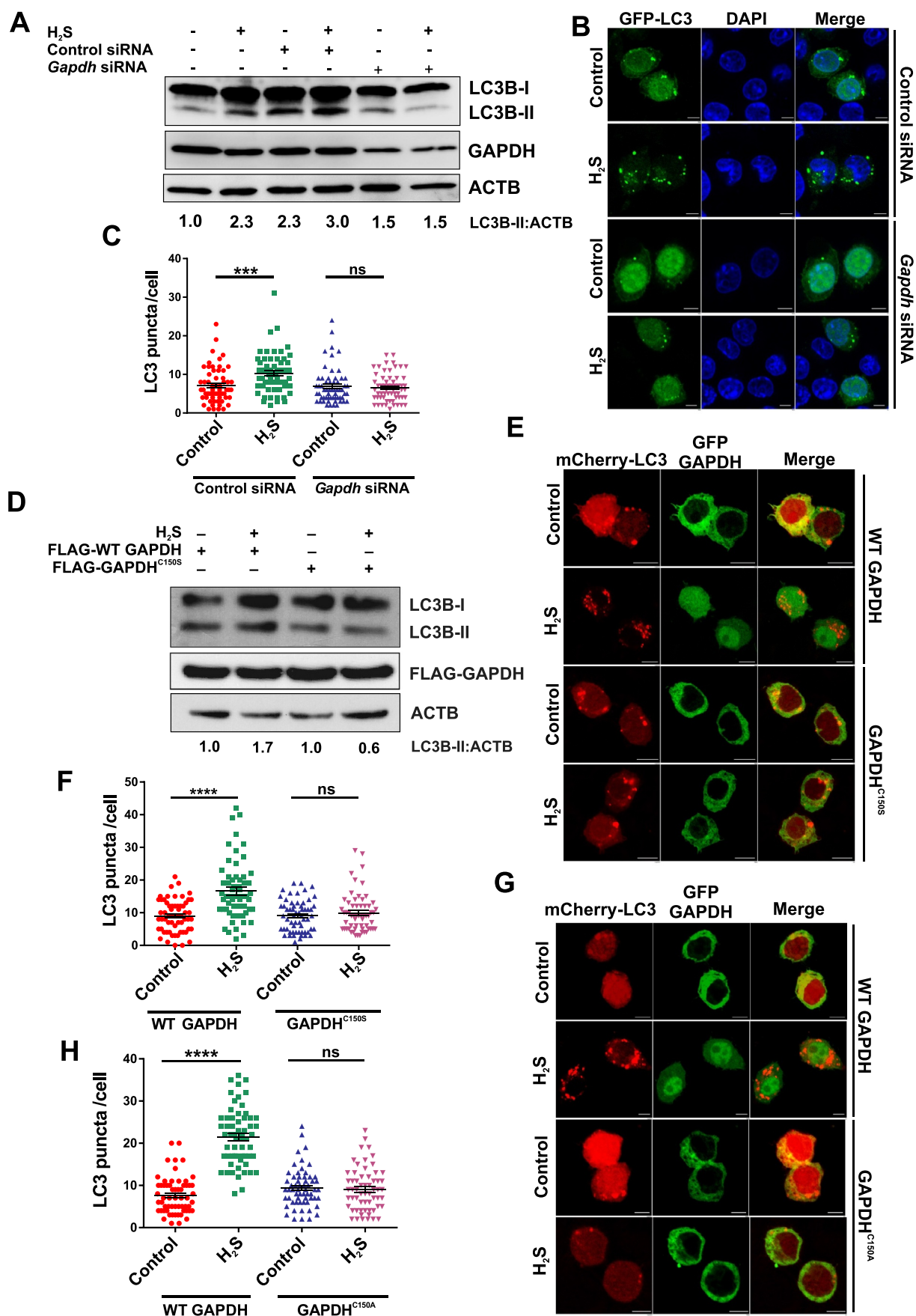


Figure 4. Sulfhydration of GAPDH active site cysteine is critical for hydrogen sulfide-induced autophagy. (A) RAW 264.7 macrophages were transfected with non-targeting siRNA or *Gapdh* siRNA. Cells were then treated with control buffer or H₂S for 2 h, and lysates were subjected to western blotting. Numbers below lanes indicate the fold change of LC3B-II relative to the ACTB signal calculated by the densitometric analysis using ImageJ. (B) RAW 264.7 macrophages were co-transfected with GFP-LC3 plasmid and non-targeting siRNA or *Gapdh* siRNA followed by treatment with H₂S for 2 h. Nuclei were counterstained with DAPI (blue) and were

imaged using confocal microscopy. (C) Quantification of cells as in (B) using ImageJ. Data represent mean \pm SEM of 3 independent experiments ($n = 60$; 20 randomly chosen cells from each experiment were quantified). Statistical significance was determined using Student's *t*-test. (D) RAW 264.7 macrophages were transiently transfected with FLAG-WT GAPDH or FLAG-GAPDH^{C150S} construct followed by treatment with control buffer or H₂S for 2 h. Lysates were prepared and subjected to western blotting. ACTB was used as a loading control, whereas FLAG-GAPDH was used as a transfection control. Numbers below lanes indicate the fold change of LC3B-II relative to the ACTB signal calculated by the densitometric analysis using ImageJ software. (E) Representative confocal images of RAW 264.7 macrophages transiently expressing mCherry-LC3 and GFP-WT GAPDH or GFP GAPDH^{C150S}. Cells were treated with H₂S for 2 h, and images were acquired using a confocal microscope. (F) Quantification of cells as in (E) using ImageJ. Data represent mean \pm SEM of 3 independent experiments ($n = 60$; 20 representative cells from each experiment were quantified). Statistical significance was determined using Student's *t*-test. (G) Representative confocal images of RAW 264.7 macrophages transiently expressing mCherry-LC3 and GFP-WT GAPDH or GFP-GAPDH^{C150A}. Cells were treated with H₂S for 2 h, and images were acquired using a confocal microscope. (H) Quantification of cells as in (G) using ImageJ. Data represent mean \pm SEM of 3 independent experiments ($n = 60$; 20 representative cells from each experiment were quantified). Statistical significance was determined using Student's *t*-test. *** indicates a *P* value of <0.001 and **** represents a *P* value of <0.0001. Scale bar: 5 μ m.

treatment with H₂S. We further analyzed whether H₂S treatment leads to a reduced interaction between SIRT1 and CCAR2 using co-immunoprecipitation experiments. Co-immunoprecipitation experiments with CCAR2 suggested that H₂S treatment reduced the interaction between CCAR2 and SIRT1 (Figure 7E and S6B), resulting in increased activity of SIRT1 as demonstrated previously with LC3, ATG7, and ATG5 as substrates. These data were verified by PLA experiments, which confirmed that treatment with H₂S leads to inhibition of the interaction between CCAR2 and SIRT1 (Figure 7F,G). Since sulfhydrylation of GAPDH plays a critical role in the translocation of GAPDH into the nucleus and H₂S increases the interaction between GAPDH and CCAR2, we next analyzed whether sulfhydrylation of GAPDH is crucial for its interaction with CCAR2. We overexpressed GAPDH^{C150S} and WT GAPDH in HEK 293 T cells and performed co-immunoprecipitation experiments to test this hypothesis. We observed a strong interaction between WT GAPDH and CCAR2 in H₂S treated cells, while no interaction was detected with the GAPDH^{C150S} mutant (Figure S6C). These observations strongly suggest that sulfhydrylation of GAPDH is critical for its interaction with CCAR2.

Discussion

H₂S activates SIRT1 and induces autophagy, but the underlying mechanism remains poorly defined. Here, we demonstrated that H₂S induces nuclear translocation of mammalian GAPDH through sulfhydrylation at its C150 residue in the active site. This nuclear translocation is critical for the induction of autophagy in response to H₂S, and the ablation of GAPDH attenuates the ability of H₂S to induce autophagy. We further demonstrated that nuclear GAPDH interacts with CCAR2 to disrupt the inhibitory interaction between CCAR2 and SIRT1. Upon activation, SIRT1 deacetylates LC3 and autophagy-related proteins, facilitating their localization from the nucleus into the cytoplasm, where they participate in autophagy. Additionally, examining the physiological relevance of H₂S-induced autophagy, we demonstrated that H₂S-induced autophagy is critical for the trafficking of *Mtb* cells into lysosomes and intracellular survival.

One of the critical findings of this study is that H₂S induced autophagy is dependent on sulfhydrylation of GAPDH. This finding establishes a crucial link between H₂S mediated protection with sulfhydrylation of GAPDH. Importantly, H₂S induces nuclear translocation of GAPDH through sulfhydrylation of active site cysteine (C150). Earlier,

Sen et al.'s elegant study demonstrated that nitrosylation at C150 (SNO-GAPDH) also results in nuclear translocation of GAPDH [39]. This nitrosylation induces the interaction of GAPDH with SIAH1, which assists in the nuclear localization of GAPDH. Sulfhydrylation of GAPDH also induces the interaction of GAPDH with SIAH1 [5], which could potentially facilitate the nuclear translocation of GAPDH. However, it must be noted that S-sulfhydrylation and S-nitrosylation have different effects on the enzymatic activity of GAPDH; S-nitrosylation inhibits [40] while S-sulfhydrylation (at C150) induces the enzymatic activity of GAPDH [4]. Furthermore, nuclear translocation associated with nitrosylation of GAPDH leads to the induction of apoptotic cell death through activation of TP53 (tumor protein p53) via histone acetyltransferase EP300/p300 (E1A binding protein p300) [39]; however, sulfhydrated GAPDH does not interact with EP300/p300 or stimulate cell death [5]. Given that NO inhibits autophagy and H₂S induces autophagy, opposing effects of NO and H₂S on the activity of GAPDH become important. Importantly, NO and H₂S also have opposing effects on SIRT1 activity. Exposure to exogenous NO inhibits the enzymatic activity of SIRT1 [7,41], while H₂S induces it [9,42]. Notably, an earlier study demonstrated that NO-mediated SIRT1 activity inhibition depends on GAPDH [7]. S-nitrosylation of GAPDH leads to the formation of SNO-GAPDH that transnitrosylates SIRT1 [7] to inhibit its activity, thereby increasing levels of acetylated TP53 for induction of apoptosis [39]. Notably, we observed that sulfhydrated GAPDH interacts with CCAR2 to release SIRT1, thereby activating SIRT1. Besides activating autophagy through deacetylation of LC3B, ATG5, and ATG7, SIRT1 could also activate autophagy through the deacetylation of FOXOs, FOXO1, and FOXO3 [43]. In the future, it will be interesting to delineate these pathways as well.

This study's significant outcome was demonstrating the interaction of sulfhydrated GAPDH with CCAR2 instead of SIRT1. This finding was surprising, albeit a critical one, and was independently confirmed using co-immunoprecipitation, pull-down assays, and PLA-based assays. Furthermore, we have demonstrated that GAPDH-CCAR2 interaction leads to the activation of SIRT1, thus the deacetylation of LC3, ATG5, and ATG7 to induce autophagy. However, activation of SIRT1 by H₂S through the pathway described in this manuscript could modulate other signaling pathways such as apoptosis through deacetylation of TP53 [44], and mitochondrial biogenesis as well as energetics through modulation of PPARGC1A [45]. We also think that the interaction of sulfhydrated GAPDH with CCAR2 could modulate other

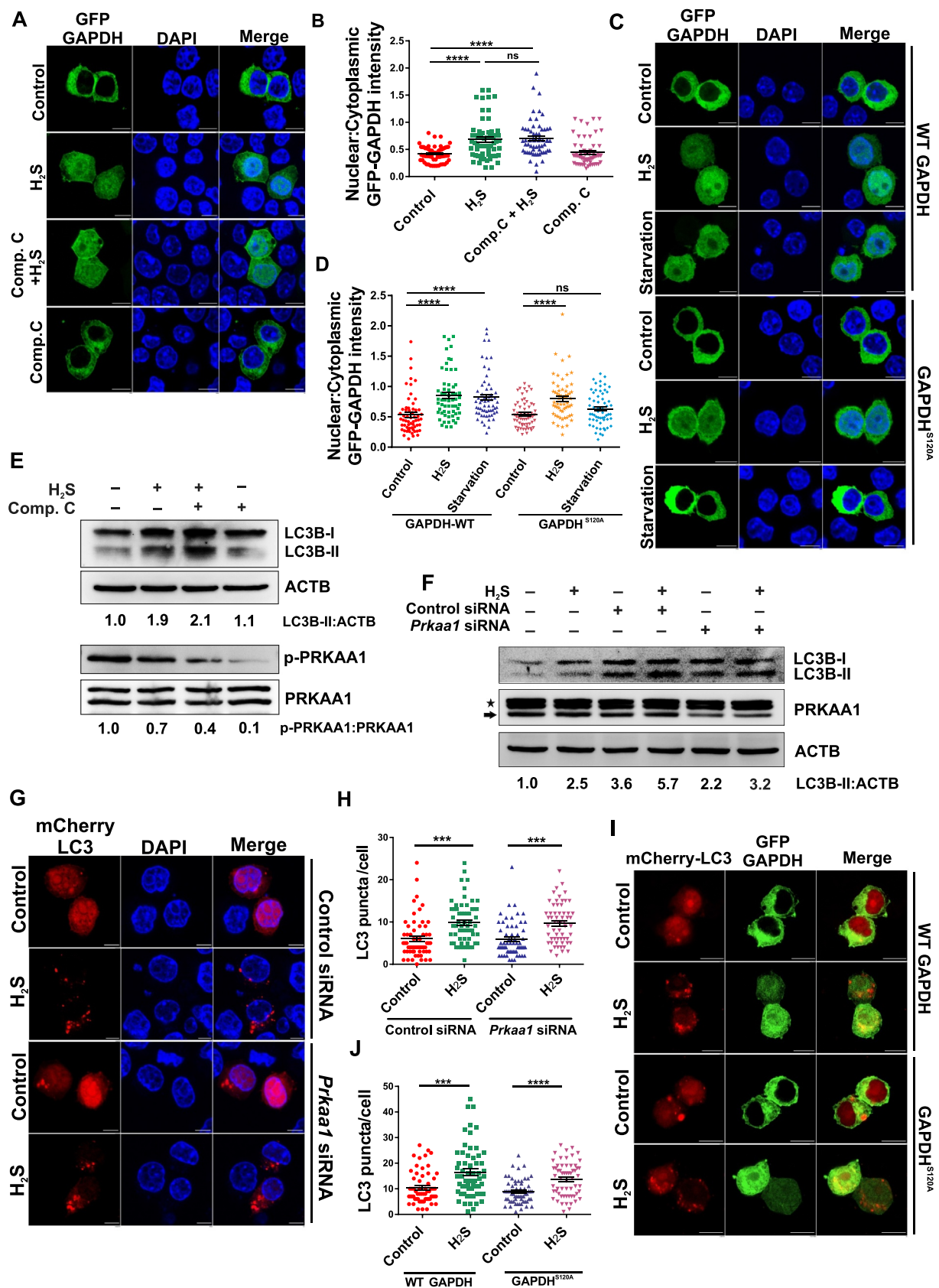


Figure 5. Hydrogen sulfide-mediated induction of autophagy does not depend upon activation of PRKAA. (A) Representative confocal images of RAW 264.7 macrophages transiently expressing GFP-GAPDH plasmid. Cells were pretreated with 10 μ M compound C for 2 h followed by treatment with H₂S for another 2 h, and images were acquired using confocal microscopy. (B) Quantification of the nuclear:cytoplasmic ratio of GAPDH in cells from the experiment (A) using ImageJ software. Data represent the mean \pm SEM from 3 independent experiments ($n = 60$; 20 randomly chosen cells from each experiment were quantified). Statistical significance was determined using Student's *t*-test. (C) Representative confocal images of RAW 264.7 macrophages transiently expressing GFP-WT GAPDH or GFP-GAPDH^{S120A} followed by treatment with H₂S or starvation for 2 h. (D) Quantification of GAPDH nuclear:cytoplasmic ratio of cells in (C) using ImageJ software. Data represent the mean \pm SEM from 3 independent experiments ($n = 60$; 20 randomly chosen cells from each experiment were quantified). Statistical significance was

determined using Student's *t*-test. (E) RAW 264.7 macrophages were pretreated with compound C (10 μ M) for 2 h, followed by treatment with H₂S for another 2 h. Cell lysates were then subjected to western blotting. Numbers below lanes indicate the fold change of LC3B-II relative to the ACTB signal and p-PRKAA1 relative to the PRKAA1 signal calculated using ImageJ software. (F) RAW 264.7 macrophages were transfected with either non-targeting siRNA or *Prkaa1* siRNA. After 48 h, cells were treated with H₂S for 2 h, and cell lysates were then subjected to western blotting. Arrow indicates the specific band of PRKAA1, while * indicates the nonspecific band. Numbers below lanes indicate the fold change of LC3B-II relative to the ACTB signal of LC3B-II relative to the ACTB signal calculated using ImageJ software. (G) RAW 264.7 macrophages were co-transfected with mCherry LC3 plasmid and non-targeting siRNA or *Prkaa1* siRNA followed by treatment with H₂S for 2 h. Nuclei were counterstained with DAPI (blue) and were imaged using confocal microscopy. (H) Quantification of cells as in (G) using ImageJ. Data represent mean \pm SEM of 3 independent experiments (n = 60; 20 randomly chosen cells from each experiment were quantified). Statistical significance was determined using Student's *t*-test. (I) Representative confocal images of RAW 264.7 macrophages transiently expressing mCherry LC3 and GFP-WT GAPDH or GFP-GAPDH^{S120A}. Cells were treated with H₂S for 2 h or control buffer, and images were acquired using confocal microscope. (J) Quantification of cells as in (I) using ImageJ. Data represent mean \pm SEM of 3 independent experiments (n = 60; 20 representative cells from each experiment were quantified). Statistical significance was determined using Student's *t*-test. *** indicates a *P* value of <0.001 and **** represents a *P* value of <0.0001. Scale bar: 5 μ m.

signaling pathways besides those wherein SIRT1 plays a role. CCAR2 interacts with epigenetic modifiers HDAC3, methyltransferase SUV39H1, and CCAR2-ZNF326 complex critical for RNA splicing [46]. Further studies are required to analyze whether H₂S modulates the function of HDAC3 and SUV39H1 through GAPDH-CCAR2 interaction. Importantly, GAPDH transnitrosylates SIRT1 [7]. However, whether GAPDH acts as a carrier for trans-S-sulfhydration of CCAR2 to alter its binding with SIRT1 or other regulators such as HDAC3 or SUV39H1 remains a potential and testable hypothesis.

The pathway delineated herein for modulation of autophagy by H₂S (summarized in Figure 8) is different than that previously described in which H₂S modulates PI3K-AKT-MTOR signaling [22] or leads to downregulation of *Mir30c*, relieving suppression of BECN1 expression [47]. Furthermore, since H₂S-mediated autophagy induction is rapid (within 20 min of exposure). Conventional pathways, such as the increase of NAD⁺, are unlikely to be critical as they take several hours to induce SIRT1 activity. We think that this pathway could be involved in H₂S-mediated health benefits wherein activation of SIRT1 plays an important role, such as vascular remodeling, cellular senescence, myocardial fibrosis, and others.

H₂S modulates mitochondrial respiration and is regarded as a regulator of cellular bioenergetics. PRKAA also regulates cellular metabolism and plays a critical role in aging [48]. Several effects mediated by H₂S are dependent upon the activation of PRKAA [49]. Recently, Chang et al. demonstrated that upon glucose starvation, PRKAA phosphorylates GAPDH at Ser122, leading to nuclear translocation of GAPDH [18]. Nuclear GAPDH directly interacts with SIRT1 to activate it [18], leading to deacetylation and export of LC3 from the nucleus [19]. Although the pathway described here for H₂S-induced GAPDH dependent autophagy bear similarities with glucose starvation-induced autophagy, there are several peculiar differences. First, H₂S-induced nuclear translocation of GAPDH is independent of PRKAA-mediated phosphorylation of GAPDH. Several lines of evidence presented in this manuscript support this conclusion, including experiments wherein genetic knockdown or pharmacological inhibition of PRKAA did not alter the induction of autophagy or nuclear translocation of GAPDH by H₂S. The observation supports these findings that H₂S induces nuclear translocation of a GAPDH (S122A) variant wherein the target site for PRKAA is mutated. It is plausible that the interaction of

sulfhydrated GAPDH with SIAH1 could play an essential role in the nuclear translocation of GAPDH.

Furthermore, H₂S induced autophagy in RAW 264.7 macrophages overexpressing a GAPDH (S122A) variant suggests that it is independent of activation of PRKAA. Second and most important is the observation that H₂S-mediated sulfhydration of GAPDH does not interact with SIRT1 but instead with CCAR2 to relieve inhibition of SIRT1. The interaction between GAPDH and CCAR2 was confirmed using PLA experiments. Given that the interaction between CCAR2 and GAPDH is novel, it will be essential to delineate the sites on GAPDH and CCAR2 involved in this interaction. Since the N-terminal domain of CCAR2 harbors a leucine zipper (LZ) motif that interacts with SIRT1 [50], it will be interesting to examine whether the same domain competitively interacts with GAPDH. It is worth noting here that unlike Chang et al. [18], we did not observe induction of autophagy upon expression of nuclear GAPDH, suggesting that nuclear localization of GAPDH alone is not sufficient to induce autophagy. This difference could arise from different cell types, for example. Chang et al. used MEFs, whereas we used RAW 264.7 macrophages. Furthermore, the inability of H₂S to induce autophagy with cells overexpressing nuclear GAPDH suggests that sulfhydration of GAPDH in the cytoplasm could facilitate yet unknown PTMs of GAPDH or interaction with some other proteins that are critical for the nuclear distribution and interaction of GAPDH with CCAR2.

The role of H₂S in TB pathogenesis has not been analyzed, although the roles of NO [51] and CO [52–54] have been studied to appreciable depths. Since we observed that H₂S induces autophagy in RAW 264.7 macrophages, we analyzed whether it relieved the inhibition of phagosome trafficking triggered by *Mtb*. We observed that H₂S facilitates the trafficking of Mb to the lysosomes and activates its killing. These findings are important in light of the availability of pharmacological donors of H₂S that are being tested in various phases of clinical trials. We further observed a critical role for SIRT1 in the autophagy-mediated clearance of *Mtb*. An earlier study supports the function of SIRT1 in TB pathogenesis, wherein activation of SIRT1 through resveratrol and SRT1720 led to restriction of intracellular *Mtb* growth [55]. Furthermore, mice with *SIRT1* deletion in the myeloid lineage were also susceptible to TB infection [55]. Additionally, the expression of SIRT1 is downregulated in TB patients. Downregulation of SIRT1 upon *Mtb* infection is also associated with TAK1 activation, enhancing the secretion of IL6 and TNF/TNF- α via the RELA/p65-MAPK/p38-MAPK/JNK-MAPK/ERK signaling axis

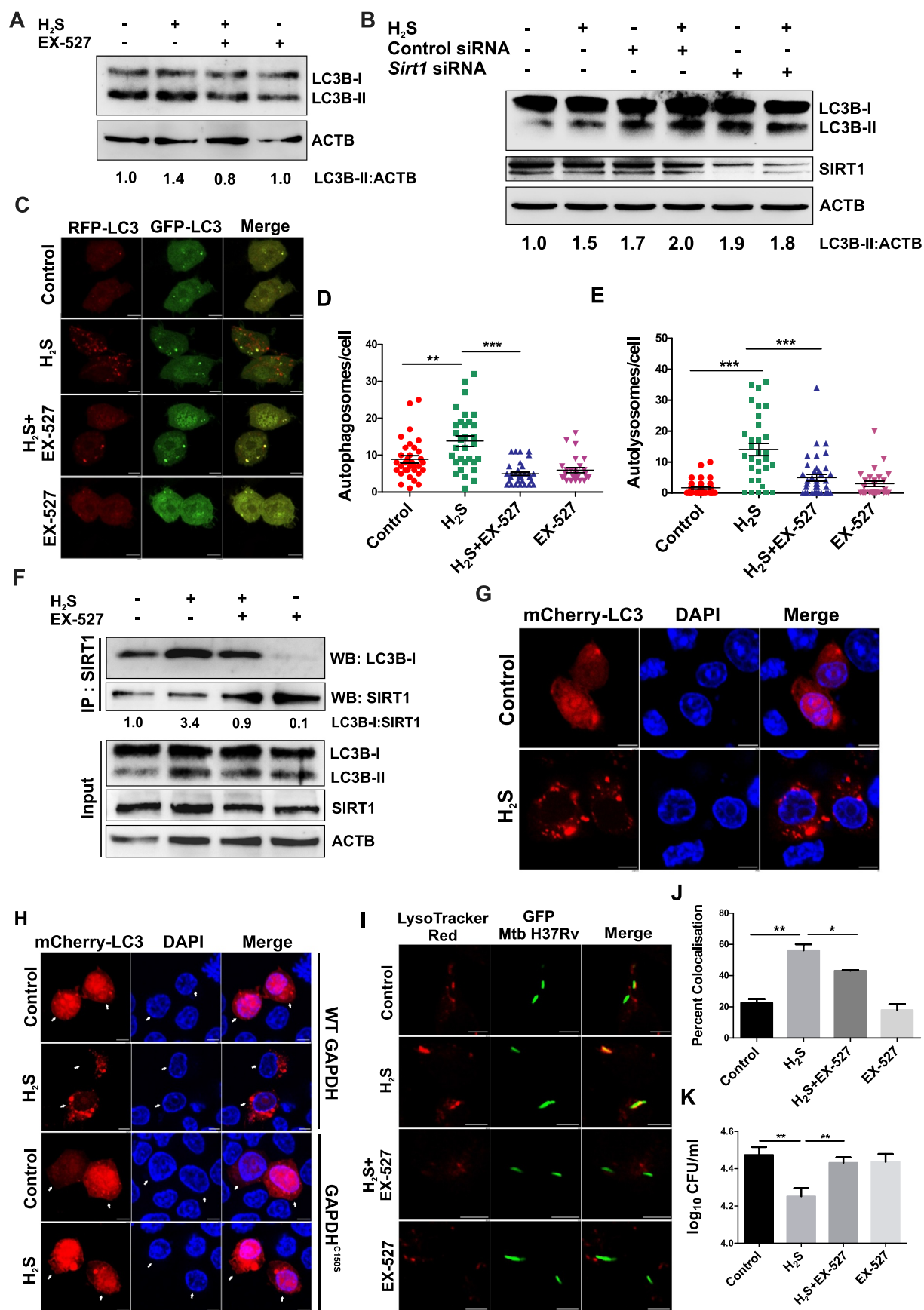


Figure 6. SIRT1 is essential for hydrogen sulfide-induced autophagy. (A) RAW 264.7 macrophages were pretreated with the SIRT1 inhibitor EX-527 (10 μ M) for 2 h, followed by treatment with H₂S for another 2 h. Cell lysates were then subjected to western blotting. Numbers below lanes indicate the fold change of LC3B-II relative to the ACTB signal calculated using the ImageJ software. (B) RAW 264.7 macrophages were transfected with either non-targeting siRNA or *SIRT1* specific siRNA. After 48 h, cells were treated with H₂S for 2 h, and lysates were subjected to western blotting. Numbers below lanes indicate the fold change of LC3B-II relative to the ACTB signal calculated using ImageJ software. (C) RAW 264.7 macrophages transiently expressing ptfLC3 construct were pretreated with 10 μ M EX-527

for 2 h followed by treatment with H₂S for another 2 h and imaged using confocal microscopy to observe autophagic flux. (D) An average number of autophagosomes per cell, as in (C), was quantified using ImageJ. (E) An average number of autolysosomes per cell, as in (C), was quantified using ImageJ. Data (in D and E) represent mean \pm SEM from 3 independent experiments (n = 60; 20 randomly chosen cells from each experiment were quantified). Statistical significance was determined using Student's *t*-test. (F) RAW 264.7 macrophages were treated as in (A), and immunoprecipitation was performed using the SIRT1 antibody followed by western blotting with LC3B or SIRT1 antibody. Numbers below lanes indicate the fold change calculated using the densitometric analysis of LC3B-1 relative to the IP:SIRT1 signal using ImageJ software. (G) Representative confocal images of RAW 264.7 macrophages transiently expressing mCherry LC3. Cells were treated with H₂S for 2 h, and images were acquired using a confocal microscope. Nuclei were stained using DAPI. (H) Representative confocal images of RAW 264.7 macrophages transiently expressing mCherry LC3 and WT GAPDH or GAPDH^{C150S}. Cells were treated with H₂S for 2 h, and images were acquired using a confocal microscope. Nuclei were stained using DAPI. Arrows represent the cells co-transfected with GFP-GAPDH and mCherry LC3. (I) Representative confocal images of RAW 264.7 macrophages infected with GFP-*Mtb* H37Rv (MOI-1:5). Cells were pretreated with 10 μ M EX-527 for 2 h, followed by treatment with H₂S for another 2 h. Lysosomes were stained using LysoTracker[®] Red, and images were acquired using confocal microscopy. (J) Percent colocalization of GFP-*Mtb* H37Rv with LysoTracker[®] Red from the result obtained in (I) was calculated using ImageJ. Data represent the mean \pm SEM from 3 independent experiments (n = 120; 40 randomly chosen *Mtb* cells from each experiment were quantified). Statistical significance was determined using Student's *t*-test. (K) *Mtb* H37Rv survival in RAW 264.7 macrophages upon 250 μ M GYY4137 treatment in the presence or absence of the SIRT1 inhibitor EX-527 (10 μ M) was analyzed using CFU estimation. Statistical significance was determined using Student's *t*-test. * indicates a *P* value of <0.05, ** indicates a *P* value of <0.01 and *** indicates a *P* value of <0.001. Scale bar: 5 μ m.

[56]. We think that further research using mouse strains defective for CSE/CBS in the myeloid lineage could improve our understanding of the role of endogenous H₂S in TB pathogenesis. However, it must be noted that several bacteria, including *Bacillus*, *Pseudomonas*, *Staphylococcus*, and *Escherichia coli*, produce H₂S, which imparts drug tolerance [57]. It would be interesting to analyze whether *Mtb* also produces H₂S and whether it protects *Mtb* from antibiotics.

In summary, the findings presented in this manuscript have delineated a novel signaling axis consisting of GAPDH-CCAR2-SIRT1-LC3. H₂S utilizes this axis for the induction of autophagy and the restriction of growth of intracellular Mycobacterium. This pathway could also play a role in other H₂S mediated health benefits wherein SIRT1 plays a critical role. This pathway could also be important for the restriction of the growth of intracellular pathogens.

Materials and methods

Plasmid constructs

pEGFP-LC3 (Addgene, 21073) [58] and ptfLC3 (Addgene, 21074) [29] were a kind gift from Tamotsu Yoshimori. mCherry-hLC3B-pcDNA3.1 was a gift from David Rubinsztein (Addgene, 40827) [59]. pEX-GFP-hLC3 Δ G was a gift from Isei Tanida (Addgene, 24988) [60]. Mouse *Gapdh* (Genbank: NM_008084.3) was cloned in pcDNA3.1 (Invitrogen, V795-20) with N-terminal GFP or C-terminal FLAG using KpnI & XhoI or HindIII & ApaI, respectively by Genscript[®] custom synthesis service. The cDNA sequences coding the NES peptide (CTTGCACTCAAGGCGGGCTTG GATATCCTTGCACTCAAGGCGGGCTTGATATCCTTGCACTCAAGGCGGGCTTGATATC) and the NLS peptide (GATCCAAAAAAGAAGAGAAAGGTAGATCCAAAAAAGAAGAGAAAGGTAGATCCAAAAAAGAAGAGAAAGGTA) were synthesized, annealed, and then inserted into GFP-GAPDH. FLAG or GFP GAPDH^{C150S} and GFP GAPDH^{S120A} were created using site directed mutagenesis. FLAG-SIRT1 (1791; deposited by Michael Greenberg's lab) and pFRT/TO/HIS/FLAG/HA-KIAA1967 (CCAR2; 38082; deposited by Markus Landthaler's lab) [61] were obtained from Addgene. CCAR2 was sub-cloned from pFRT/TO/HIS/FLAG/HA-KIAA1967 into pcDNA3.1- N-terminal FLAG tagged

plasmid. GW1-PercevalHR, probe for ATP measurement: ADP ratio was a kind gift from Gary Yellen (Addgene, 49082) [38].

Antibodies and reagents

The antibodies for LC3B (2775), ATG5 (12994), ATG7 (8558 c) and PRKAA1 (2532) were obtained from Cell Signaling Technology (CST). ACTB (A5441) and anti-FLAG (F1804) antibodies were from Sigma Aldrich. Antibodies against LMNB1 (ab133741), CCAR2 (ab70239), SIRT1 (ab12193), GAPDH (ab181602), PRKAA1 (ab80039), and p-PRKAA1 (ab133448) were purchased from Abcam. Antibodies used for the proximity ligation assay (PLA) were CCAR2 (CST, 5857), GAPDH (Abcam, ab181602), and SIRT1 (Abcam, ab12193). Alexa Fluor 488 (A11034) and 647 (A21245)-tagged secondary antibodies for immunostaining were from Molecular Probes, Invitrogen. Anti rabbit-HRP-labeled secondary antibody was obtained from Santa Cruz Biotechnology (sc 2357) and anti-mouse HRP-labeled secondary antibody (A9044) obtained from Sigma Aldrich. Anti-FLAG beads were procured from Sigma Aldrich (A2220).

GYY4137 was procured from Cayman Chemicals (13345). LysoTracker Red DND 99 (L7528), DQ[™] Red BSA, Lipofectamine 3000 (L3000001), Dulbecco's Modified Eagle Medium (DMEM, 10569010), fetal bovine serum (the United States, certified,16000044), and Pierce[™] Co-Immunoprecipitation Kit (26149) were purchased from Thermo Fisher Scientific

Cell culture, transfection, and treatment

RAW 264.7 cells obtained from ATCC (ATCC[®], TIB-71) were grown in Dulbecco's modified Eagle's medium supplemented with 10% fetal bovine serum at 37°C under 5% CO₂. WT MEFs (ATCC[®], CRL-2991[™]), 293/HEK293 (ATCC[®], CRL-1573), and 293 T (ATCC[®], CRL-3216[™]) cells were cultured at 37°C in DMEM supplemented with 10% fetal bovine serum and non-essential amino acids. Transient transfections were performed using Lipofectamine 3000 according to the manufacturer's instructions. Cells were analyzed 18–24 h after transfection.

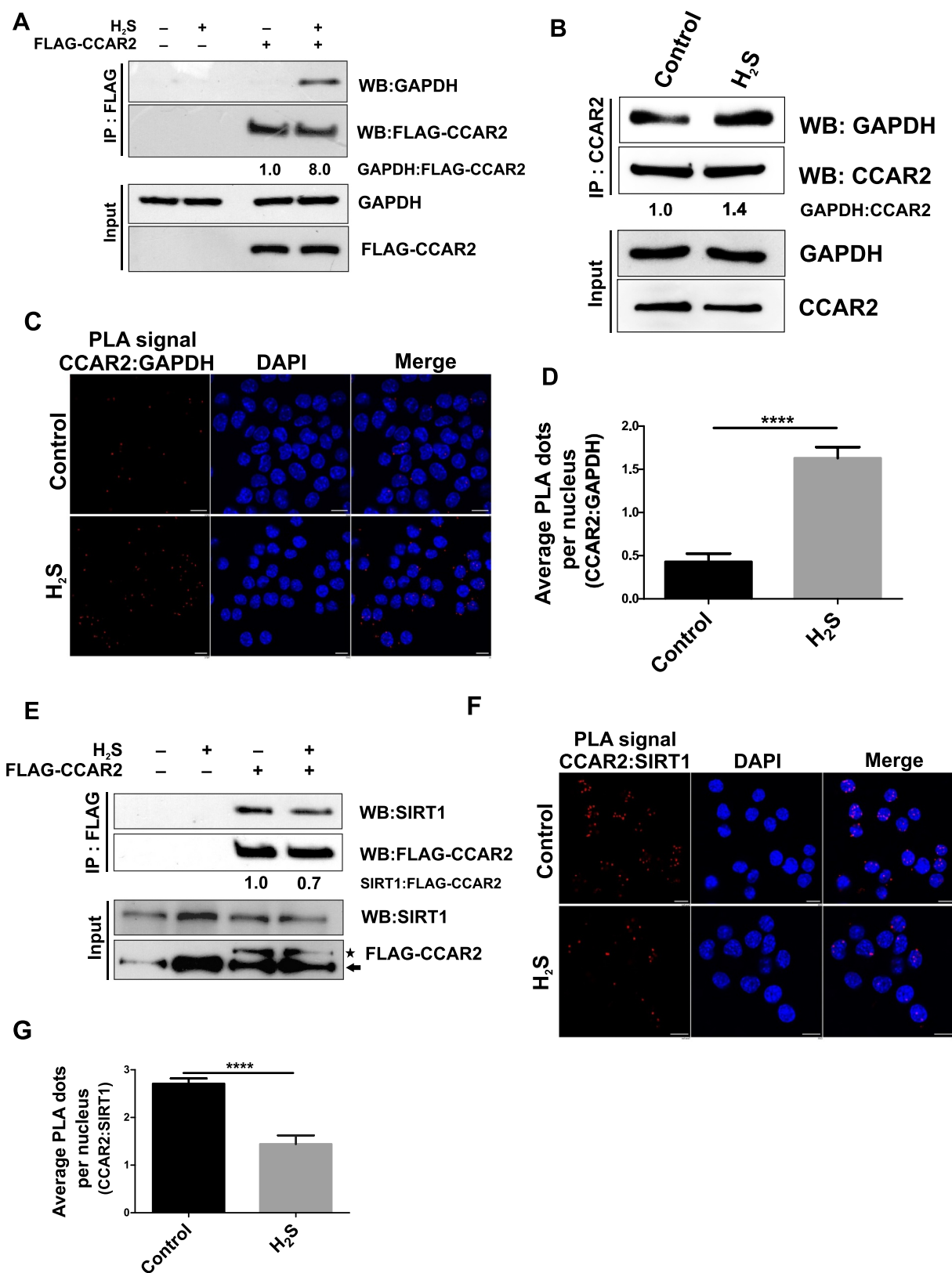


Figure 7. Hydrogen sulfide induces the interaction of GAPDH with CCAR2. (A) HEK 293 cells overexpressing FLAG-CCAR2 were treated with H₂S for 2 h and subjected to immunoprecipitation using FLAG beads. Western blotting was performed using anti-GAPDH and anti-FLAG antibodies. Numbers below lanes indicate the fold change of GAPDH relative to the IP:FLAG-CCAR2 signal calculated using the ImageJ software. (B) HEK 293 cells were treated with H₂S for 2 h and subjected to immunoprecipitation using anti-CCAR2 antibody. Western blotting was performed using anti-GAPDH and anti-CCAR2 antibodies. Numbers below lanes indicate the fold change of GAPDH relative to the IP:CCAR2 signal calculated using the ImageJ software. (C) Representative confocal images of RAW 264.7 macrophages after *in situ* proximity ligation assay (PLA). Anti-GAPDH and anti-CCAR2 antibodies were used for the *in situ* PLA. (D) Quantification of PLA dots per nucleus from cells in (C). Data (mean \pm SEM) are representative of three independent experiments performed in triplicate. Statistical significance was determined using Student's *t*-test. (E) HEK 293 cells overexpressing FLAG-CCAR2 were treated with H₂S for 2 h, and immunoprecipitation was performed using anti-FLAG beads. Western blotting was performed to measure coimmunoprecipitated SIRT1. In the input image, arrow indicates a nonspecific band while * indicates the specific band of CCAR2. Numbers below lanes indicate the fold change of SIRT1 relative to the IP:FLAG-CCAR2 signal calculated using the ImageJ software. (F) Representative confocal images of RAW

264.7 macrophages after *in situ* PLA. Anti-CCAR2 and anti-SIRT1 antibodies were used for the *in situ* PLA. (G) Quantification of PLA dots per nucleus from cells in (F). Data (mean \pm SEM) are representative of three independent experiments performed in triplicate. Statistical significance was determined using Student's *t*-test. *** indicates a *P* value of <0.001 . Scale bars: 10 μ m.

According to the manufacturer's protocol for RNA interference, siRNA duplexes were transfected using Lipofectamine 3000 for 48 h. *Sirt1* (DIRME-000037) siRNA UGAAGUGCCUCAGAUUUAdTdT) was custom synthesized from Dharmacon. The mission esiRNAs for *Gapdh* (EMU184491) and *Prkaa1* (EMU190491) were obtained from Sigma Aldrich. Non-targeting siRNA was from Dharmacon.

For H₂S exposure, cells were treated with 500 μ M GYY4137 for 2 h. For starvation, cells were washed twice with PBS (NaCl [Sigma Aldrich, S8776], KCl [Sigma Aldrich, 60128-1 KG], Na₂HPO₄ [Sigma Aldrich, S3264-1 KG], KH₂PO₄ [Sigma Aldrich, P5655-500 G], pH 7.4) and then incubated with EBSS for 2 h. Other treatments- EX-527 (Sigma Aldrich, E7034) 10 μ M for 2 h, wortmannin (Sigma Aldrich, W3144) 10 μ M for 1 h, bafilomycin A₁ (Sigma Aldrich, B1793) 100 nM for 2 h, compound C (Merck Millipore, 171261) 10 μ M for 2 h.

Immunostaining and confocal microscopy

For immunostaining, cells were fixed in 4% paraformaldehyde for 10 min at room temperature, followed by permeabilization and blocking with PBS containing 3% BSA (HIMEDIA, MB083) and 0.1% saponin (Sigma Aldrich, 84510) for 30 min. The cells were then incubated for 1 h at room temperature with the antibodies indicated in figure legends, followed by incubation with appropriate secondary antibodies. Images were acquired on a Nikon A1R using scanning confocal microscope mode and analyzed with the ImageJ Software.

Western blot and immunoprecipitation

Following the treatments, the cells were washed with DPBS (Thermo Fischer, 140190144), and the lysate was prepared in RIPA buffer (Cell Signaling Technology, 9806) with a protease inhibitor cocktail (Roche, 589270001). The protein concentration was estimated using the BCA kit containing BCA solution (B9643) and CuSO₄ (C2284) from Sigma Aldrich, and the samples were subjected to SDS-PAGE followed by transfer to a PVDF membrane (MDI Membrane Technologies, SVFX8301XXXX101). Blots were developed using HRP-conjugated secondary antibodies. Blots were developed using enhanced chemiluminescence (ECL)-Luminata forte (Merck, WBLUF0500) and exposed to X ray retina film (XBE X ray film, 6574958) for visualization of bands. Otherwise, digital images were acquired using the ImageQuant LAS 4000 (GE healthcare bioscience).

For immunoprecipitation, cells were lysed in lysis buffer (50 mM Tris [Invitrogen, AM9850G], pH 7.0, 150 mM NaCl [Invitrogen, AM9759], 1 mM EDTA [Invitrogen, AM9260G], 1% Triton X-100 [Sigma Aldrich, 78787]) containing protease inhibitor cocktail and incubated with anti-FLAG beads (Sigma Aldrich, A2220) or primary antibody coupled with Amino linked beads (Pierce, 26149) for overnight at 4°C. Co-Immunoprecipitation was performed according to the manufacturer's protocol using the FLAG Co-IP kit or amino link Co-IP kit. Immunocomplexes were separated by SDS-PAGE and detected with western blot.

Subcellular fractionation

Nuclear and cytoplasmic fractions were isolated, as previously described [62]. Briefly, after treatment, the cells were washed

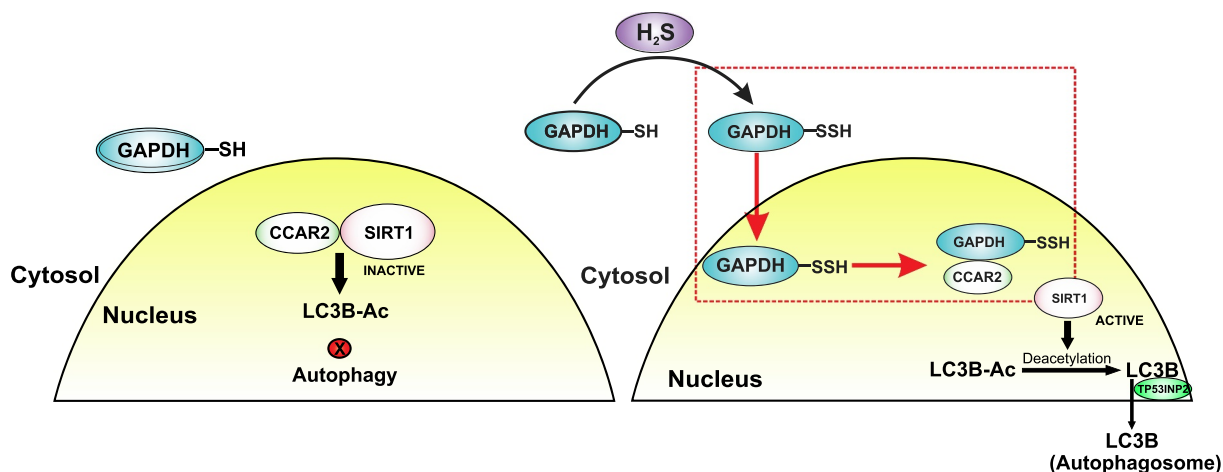


Figure 8. Model depicting the mechanism of hydrogen sulfide mediated activation of autophagy. Under resting conditions (panel i), SIRT1 is inhibited by CCAR2. Exogenous or endogenous hydrogen sulfide leads to sulfhydrylation of active site cysteine, which guides the nuclear translocation of GAPDH (panel ii). Nuclear GAPDH interacts with CCAR2 leading to disruption of the SIRT1-CCAR2 complex and activation of SIRT1. Activation of SIRT1 results in the deacetylation of LC3B, ATG5, and ATG7 and their redistribution to the cytoplasm and, thus, activation of autophagy. Pathway highlighted using the red arrow and red box are the novel findings of this study.

twice with PBS and lysed in cytosol buffer containing 50 mM HEPES, pH 7.4, 150 mM NaCl, and 25 µg/ml digitonin (Sigma Aldrich, D141) supplemented with protease inhibitor cocktail. The lysate was centrifuged at 7000 X g, 10 min to pellet the nuclei. The supernatant contained the cytosolic fraction, and the pellet was washed twice with PBS to remove any cytosolic fraction. The pellet was resuspended in a nuclear buffer composed of 50 mM HEPES, pH 7.4, 150 mM NaCl, 0.5% sodium deoxycholate (Sigma Aldrich, 30970), 0.1% SDS (Sigma Aldrich, L5750), 1 U/ml benzonase (Sigma Aldrich, E8263), and protease inhibitor cocktail followed by incubation with end-to-end mixing at 4°C for overnight. The supernatant obtained after centrifugation at 7000 X g, 10 min represented the nuclear fraction.

LysoTracker® red staining

For LysoTracker® Red staining, after 3 h of GFP-*Mtb* H37Rv infection, the cells were washed and treated as indicated in the figure legends. After the treatment, the cells were stained with 150 nM of LysoTracker Red DND99 for 20 min, followed by washing with PBS and slide preparation. 488-nm and 561-nm laser sources were used for detecting GFP-*Mtb* H37Rv and LysoTracker® Red, respectively.

Colony-forming unit assay

RAW 264.7 macrophages (0.5×10^6) were plated in a 6-well plate. The cells were infected with *Mtb* H37Rv (1:10 multiplicity of infection [MOI]) for 3 h and treated as indicated in the figure legends. The cells were lysed with 0.06% SDS after 72 h, serially diluted, and plated on Middlebrook 7H11 (Becton Dickinson, Difco, 212203) plates supplemented with 10% OADC (NaCl [Sigma Aldrich Aldrich, S8776], Dextrose [Merck Millipore, QD5P65116], BSA fraction V [HIMEDIA, GRM105], Catalase [Sigma Aldrich, C1345] and Oleic acid [Sigma Aldrich, 01008]). The plates were incubated at 37°C, and the *Mtb* colonies were counted after 2 to 3 weeks.

Proximity ligation assay

Cells were treated as described and fixed using 4% paraformaldehyde (Sigma Aldrich, 158122). This was followed by permeabilization using 0.1% saponin for 5 min. The in-situ proximity ligation was performed according to the manufacturer's protocol (Sigma Aldrich, DUO92004), and images were captured using a confocal microscope (A1R; Nikon). PLA signals were quantified using ImageJ.

Modified biotin switch assay

The assay was carried out, as described previously [4]. Briefly, cells treated were lysed in HEN buffer (250 mM HEPES, pH 7.7, 1 mM EDTA, and 0.1 mM neocuproine [Sigma Aldrich, N1501]) supplemented with protease and phosphatase (Roche, 589270001) inhibitor. The Cell lysates were added to the blocking buffer (HEN buffer adjusted to 2.5% SDS and 20 mM MMTS [Thermo Fischer, 23011]) at 50°C for 20 min with mixing at 394 X g. The MMTS was then removed by

acetone precipitation. After acetone removal, the proteins were resuspended in HENS buffer (HEN buffer adjusted to 1% SDS) containing 0.8 mM biotin-HPDP (Thermo Fischer, 21341) and incubated for two h at room temperature. Biotinylated proteins were affinity isolated using streptavidin agarose beads (Sigma Aldrich, E5529), followed by washing with HENS buffer. The biotinylated proteins were eluted by adding SDS-PAGE sample buffer and subjected to western blot analysis. For quantification of GAPDH sulphydration, samples were run on blots alongside total lysates and subjected to immunoblotting with GAPDH.

Protein persulphide detection protocol (ProPerDP)

Protein sulphydration was detected by using the earlier described method [36]. HEK293T cells were seeded in 90-mm dishes and transfected with FLAG-WT GAPDH and FLAG-GAPDH^{C150S} vector using Lipofectamine 3000 according to the manufacturer's protocol. Briefly, cells were treated with 100 µM of sodium hydrogen sulfide (hydrate) (Cayman Chemical, 10012555) for 2 h at 37°C. Cells were washed with PBS and incubated with 1 mM EZ-link-Iodoacetyl-PEG₂-Biotin (Sigma Aldrich, 21334) for 3 h at 37°C. The cells were washed twice with PBS and lysed using lysis buffer (40 mM HEPES [Sigma Aldrich, H3375], 50 mM NaCl, 1 mM EGTA [Sigma Aldrich, E8145], 1 mM EDTA, pH 7.4, 1% CHAPS [Sigma Aldrich, C9426]) containing 1% protease inhibitor cocktail. Biotinylated proteins were pulled down using streptavidin agarose beads followed by washing with lysis buffer to remove unbound proteins. The biotinylated protein was eluted using 25 mM dithiothreitol (Sigma Aldrich, 43815) and subjected to western blotting with anti-FLAG antibody (CST, 2368).

ANXA5/annexin V-7AAD staining

FITC-conjugated ANXA5/annexin V (Invitrogen, V13241) and 7AAD (Invitrogen, A1310) staining were performed as per the manufacturer protocol to detect apoptotic cell population. Briefly, RAW 264.7 cells were seeded in a 6-well plate and treated with 500 µM GYY4137 for 7 h. After treatment, cells were washed with PBS twice and detached using PBS-EDTA. Afterward, cells were washed with 1X ANXA5/annexin V binding buffer and stained with ANXA5/annexin V-FITC for 15 min, followed with 7AAD staining for 5 min in the dark, at room temperature. The apoptotic population (ANXA5⁺ 7AAD^{-/+}) was determined by acquiring the samples using the BD-FACS verse cell analyzer. Data were analyzed using FACS-verse software.

Culturing mycobacterium

Mtb H37Rv (ATCC, 27294) and GFP-*Mtb* H37Rv were cultured in 7H9 medium (Becton Dickinson, Difco, 271310) with 0.1% Tween 80 (MP Biomedicals, 103170) and 10% Middlebrook OADC enrichment until the optical density at 600 nm reached 0.8 to 1.0. The culture was then centrifuged at 1811 X g for 10 min, and the pellet was suspended in a freezing medium (complete 7H9 medium + 20% glycerol). Colony-

forming unit (CFU) plating was performed to estimate the number of viable cells, and the stocks were prepared and stored at -80°C . These stocks were used for all the experiments. All experiments involving *Mtb* H37Rv were conducted in a BSL-3/A-BSL-3 facility at CSIR-IMTech, Chandigarh.

DQ™ Red BSA staining

Following the infection of RAW 264.7 cells with GFP-*Mtb* H37Rv, cells were pulsed with DQ™ Red BSA for 20 min and washed to remove the excess. Cells were treated as indicated in the figure legends and fixed using 4% paraformaldehyde. Images were acquired using Nikon A1R confocal laser scanning microscope.

Statistical analysis

All the statistical data are presented as mean \pm SEM from at least three independent experiments. The statistical significance of differences was determined using GraphPad Prism v6.04 (GraphPad Software Inc., USA) by applying Student's *t*-test. $p < 0.05$ was considered to be statistically significant.

Acknowledgments

This work was supported by a research grant (BT/PR30745/MED/29/1366/2018) from the Department of Biotechnology, Govt. of India. AK is supported through "Swarnajayanti Fellowship 2016-2017" and "National Bioscience Award for Career Development 2017/2018" by the Department of Science and Technology and Department of Biotechnology, Govt. of India, respectively. IKI and SB are supported by a senior research fellowship from the Council of Scientific and Industrial Research. SS is supported by a senior research fellowship from the Department of Biotechnology. We are thankful to Mr. Rajkumar, CSIR-Institute of Microbial Technology, for the management of laboratory requirements.

Disclosure statement

The authors declare that they do not have any competing financial interests.

Funding

This work was supported by the Department of Biotechnology, Ministry of Science and Technology [BT/PR30745/MED/29/1366/2018].

ORCID

Ashwani Kumar  <http://orcid.org/0000-0002-6240-6810>

References

- Li L, Rose P, Moore PK. Hydrogen sulfide and cell signaling. *Annu Rev Pharmacol Toxicol.* 2011;51(1):169–187.
- Paul BD, Snyder SH. H₂S : a novel gasotransmitter that signals by sulfhydrylation. *Trends Biochem Sci.* 2015;40(11):687–700.
- Paul BD, Snyder SH. H(2)S signalling through protein sulfhydrylation and beyond. *Nat Rev Mol Cell Biol.* 2012;13(8):499–507.
- Mustafa AK, Gadalla MM, Sen N, et al. H₂S signals through protein S-sulfhydrylation. *Sci Signal.* 2009;2:ra72.
- Mir S, Sen T, Sen N. Cytokine-induced GAPDH sulfhydrylation affects PSD95 degradation and memory. *Mol Cell.* 2014;56:786–795.
- Hara MR, Agrawal N, Kim SF, et al. S-nitrosylated GAPDH initiates apoptotic cell death by nuclear translocation following Siah1 binding. *Nat Cell Biol.* 2005;7:665–674.
- Kornberg MD, Sen N, Hara MR, et al. GAPDH mediates nitrosylation of nuclear proteins. *Nat Cell Biol.* 2010;12:1094–1100.
- Li X, Zhang KY, Zhang P, et al. Hydrogen sulfide inhibits formaldehyde-induced endoplasmic reticulum stress in PC12 cells by upregulation of SIRT-1. *PLoS One.* 2014;9:e89856.
- Suo R, Zhao ZZ, Tang ZH, et al. Hydrogen sulfide prevents H(2)O (2)-induced senescence in human umbilical vein endothelial cells through SIRT1 activation. *Mol Med Rep.* 2013;7:1865–1870.
- Rahman S, Islam R. Mammalian Sirt1: insights on its biological functions. *Cell Commun Signal.* 2011;9(1):11.
- Deretic V, Levine B. Autophagy, immunity, and microbial adaptations. *Cell Host Microbe.* 2009;5(6):527–549.
- Deretic V, Saitoh T, Akira S. Autophagy in infection, inflammation and immunity. *Nat Rev Immunol.* 2013;13(10):722–737.
- Bradfute SB, Castillo EF, Arko-Mensah J, et al. Autophagy as an immune effector against tuberculosis. *Curr Opin Microbiol.* 2013;16(3):355–365.
- Castillo EF, Dekonenko A, Arko-Mensah J, et al. Autophagy protects against active tuberculosis by suppressing bacterial burden and inflammation. *Proc Natl Acad Sci U S A.* 2012;109(46):E3168–76.
- Deretic V, Delgado M, Vergne I, et al. Autophagy in immunity against mycobacterium tuberculosis: a model system to dissect immunological roles of autophagy. *Curr Top Microbiol Immunol.* 2009;335:169–188.
- Singh N, Kansal P, Ahmad Z, et al. Antimycobacterial effect of IFNG (interferon gamma)-induced autophagy depends on HMOX1 (heme oxygenase 1)-mediated increase in intracellular calcium levels and modulation of PPP3/calceurin-TFEB (transcription factor EB) axis. *Autophagy.* 2018;14(6):972–991.
- Mizushima N. Autophagy: process and function. *Genes Dev.* 2007;21(22):2861–2873.
- Chang C, Su H, Zhang D, et al. AMPK-dependent phosphorylation of GAPDH triggers Sirt1 activation and is necessary for autophagy upon glucose starvation. *Mol Cell.* 2015;60(6):930–940.
- Huang R, Xu Y, Wan W, et al. Deacetylation of nuclear LC3 drives autophagy initiation under starvation. *Mol Cell.* 2015;57(3):456–466.
- Wang D, Ma Y, Li Z, et al. The role of AKT1 and autophagy in the protective effect of hydrogen sulphide against hepatic ischemia/reperfusion injury in mice. *Autophagy.* 2012;8(6):954–962.
- Sun L, Zhang S, Yu C, et al. Hydrogen sulfide reduces serum triglyceride by activating liver autophagy via the AMPK-mTOR pathway. *Am J Physiol Endocrinol Metab.* 2015;309(11):E925–35.
- Wang SS, Chen YH, Chen N, et al. Hydrogen sulfide promotes autophagy of hepatocellular carcinoma cells through the PI3K/Akt/mTOR signaling pathway. *Cell Death Dis.* 2017;8(3):e2688.
- Xie L, Yu S, Yang K, et al. Hydrogen sulfide inhibits autophagic neuronal cell death by reducing oxidative stress in spinal cord ischemia reperfusion injury. *Oxid Med Cell Longev.* 2017;2017:8640284.
- Jiang H, Xiao J, Kang B, et al. PI3K/SGK1/GSK3beta signaling pathway is involved in inhibition of autophagy in neonatal rat cardiomyocytes exposed to hypoxia/reoxygenation by hydrogen sulfide. *Exp Cell Res.* 2016;345(2):134–140.
- Song ZJ, Ng MY, Lee Z-W, et al. Hydrogen sulfide donors in research and drug development. *Med Chem Comm.* 2014;5(5):557–570.
- Zaorska E, Tomasova L, Koszelewski D, et al. Hydrogen sulfide in pharmacotherapy, beyond the hydrogen sulfide-donors. *Biomolecules.* 2020;10:323.
- Li L, Whiteman M, Guan YY, et al. Characterization of a novel, water-soluble hydrogen sulfide-releasing molecule (GYY4137):

- new insights into the biology of hydrogen sulfide. *Circulation*. 2008;117(18):2351–2360.
- [28] Mizushima N, Yoshimori T. How to interpret LC3 immunoblotting. *Autophagy*. 2007;3(6):542–545.
- [29] Kimura S, Noda T, Yoshimori T. Dissection of the autophagosome maturation process by a novel reporter protein, tandem fluorescent-tagged LC3. *Autophagy*. 2007;3(5):452–460.
- [30] Tanida I, Ueno T, Kominami E. Human light chain 3/ MAP1LC3B is cleaved at its carboxyl-terminal Met121 to expose Gly120 for lipidation and targeting to autophagosomal membranes. *J Biol Chem*. 2004;279(46):47704–47710.
- [31] Hong Y-S, Ham Y-A, Choi J-H, et al. Effects of allyl sulfur compounds and garlic extract on the expression of Bcl-2, Bax, and p53 in non small cell lung cancer cell lines. *Exp Mol Med*. 2000;32(3):127–134.
- [32] Klionsky DJ, Abdelmohsen K, Abe A, et al. Guidelines for the use and interpretation of assays for monitoring autophagy (3rd edition). *Autophagy*. 2016;12:1–222.
- [33] Gutierrez MG, Master SS, Singh SB, et al. Autophagy is a defense mechanism inhibiting BCG and Mycobacterium tuberculosis survival in infected macrophages. *Cell*. 2004;119:753–766.
- [34] Pilli M, Arko-Mensah J, Ponpuak M, et al. TBK-1 promotes autophagy-mediated antimicrobial defense by controlling autophagosome maturation. *Immunity*. 2012;37:223–234.
- [35] Manzanillo PS, Ayres JS, Watson RO, et al. The ubiquitin ligase parkin mediates resistance to intracellular pathogens. *Nature*. 2013;501:512–516.
- [36] Doka E, Pader I, Biro A, et al. A novel persulfide detection method reveals protein persulfide- and polysulfide-reducing functions of thioredoxin and glutathione systems. *Sci Adv*. 2016;2:e1500968.
- [37] Leustek T, Martin MN, Bick JA, et al. Pathways and regulation of sulfur metabolism revealed through molecular and genetic studies. *Ann Rev Plant Physiol Plant Mol Biol*. 2000;51:141–165.
- [38] Tantama M, Martinez-Francois JR, Mongeon R, et al. Imaging energy status in live cells with a fluorescent biosensor of the intracellular ATP-to-ADP ratio. *Nat Commun*. 2013;4:2550.
- [39] Sen N, Hara MR, Kornberg MD, et al. Nitric oxide-induced nuclear GAPDH activates p300/CBP and mediates apoptosis. *Nat Cell Biol*. 2008;10:866–873.
- [40] Molina Y Vedia L, McDonald B, Reep B, et al. Nitric oxide-induced S-nitrosylation of glyceraldehyde-3-phosphate dehydrogenase inhibits enzymatic activity and increases endogenous ADP-ribosylation. *J Biol Chem*. 1992;267:24929–24932.
- [41] Shinozaki S, Chang K, Sakai M, et al. Inflammatory stimuli induce inhibitory S-nitrosylation of the deacetylase SIRT1 to increase acetylation and activation of p53 and p65. *Sci Signal*. 2014;7:ra106.
- [42] Xin H, Wang M, Tang W, et al. Hydrogen sulfide attenuates inflammatory hepcidin by reducing IL-6 secretion and promoting SIRT1-mediated STAT3 deacetylation. *Antioxid Redox Signal*. 2016;24:70–83.
- [43] Ng F, Tang BL. Sirtuins' modulation of autophagy. *J Cell Physiol*. 2013;228:2262–2270.
- [44] Busch F, Mobasher A, Shayan P, et al. Sirt-1 is required for the inhibition of apoptosis and inflammatory responses in human tenocytes. *J Biol Chem*. 2012;287:25770–25781.
- [45] Nemoto S, Fergusson MM, Finkel T. SIRT1 functionally interacts with the metabolic regulator and transcriptional coactivator PGC-1{alpha}. *J Biol Chem*. 2005;280:16456–16460.
- [46] Chini EN, Chini CC, Nin V, et al. Deleted in breast cancer-1 (DBC-1) in the interface between metabolism, aging and cancer. *Biosci Rep*. 2013;33(4):637–643.
- [47] Li L, Jiang HK, Li YP, et al. Hydrogen sulfide protects spinal cord and induces autophagy via miR-30c in a rat model of spinal cord ischemia-reperfusion injury. *J Biomed Sci*. 2015;22:50.
- [48] Burkewitz K, Zhang Y, Mair WB. AMPK at the nexus of energetics and aging. *Cell Metab*. 2014;20:10–25.
- [49] Wang M, Tang W, Zhu YZ. An update on AMPK in hydrogen sulfide pharmacology. *Front Pharmacol*. 2017;8:810.
- [50] Kim JE, Chen J, Lou Z. DBC1 is a negative regulator of SIRT1. *Nature*. 2008;451:583–586.
- [51] MacMicking JD, North RJ, LaCourse R, et al. Identification of nitric oxide synthase as a protective locus against tuberculosis. *Proc Natl Acad Sci U S A*. 1997;94:5243–5248.
- [52] Kumar A, Deshane JS, Crossman DK, et al. Heme oxygenase-1-derived carbon monoxide induces the Mycobacterium tuberculosis dormancy regulon. *J Biol Chem*. 2008;283:18032–18039.
- [53] Kumar A, Toledo JC, Patel RP, et al. Mycobacterium tuberculosis DosS is a redox sensor and DosT is a hypoxia sensor. *Proc Natl Acad Sci U S A*. 2007;104:11568–11573.
- [54] Singh N, Ahmad Z, Baid N, et al. Host heme oxygenase-1: friend or foe in tackling pathogens? *IUBMB Life*. 2018;70:869–880.
- [55] Cheng CY, Gutierrez NM, Marzuki MB, et al. Host sirtuin 1 regulates mycobacterial immunopathogenesis and represents a therapeutic target against tuberculosis. *Sci Immunol*. 2017;2:eaaj1789:1–12.
- [56] Yang H, Hu J, Chen YJ, et al. Role of Sirt1 in innate immune mechanisms against Mycobacterium tuberculosis via the inhibition of TAK1 activation. *Arch Biochem Biophys*. 2019;667:49–58.
- [57] Shatalin K, Shatalina E, Mironov A, et al. H2S: a universal defense against antibiotics in bacteria. *Science*. 2011;334:986–990.
- [58] Kabeya Y, Mizushima N, Ueno T, et al. LC3, a mammalian homologue of yeast Apg8p, is localized in autophagosome membranes after processing. *Embo J*. 2000;19:5720–5728.
- [59] Jahreiss L, Menzies FM, Rubinsztein DC. The itinerary of autophagosomes: from peripheral formation to kiss-and-run fusion with lysosomes. *Traffic*. 2008;9:574–587.
- [60] Tanida I, Yamaji T, Ueno T, et al. Consideration about negative controls for LC3 and expression vectors for four colored fluorescent protein-LC3 negative controls. *Autophagy*. 2008;4:131–134.
- [61] Baltz AG, Munschauer M, Schwanhausser B, et al. The mRNA-bound proteome and its global occupancy profile on protein-coding transcripts. *Mol Cell*. 2012;46:674–690.
- [62] Holden P, Horton WA. Crude subcellular fractionation of cultured mammalian cell lines. *BMC Res Notes*. 2009;2:243.